Topological gapless phases in nonsymmorphic antiferromagnets

Wojciech Brzezicki and Mario Cuoco
CNR-SPIN, IT-84084 Fisciano (SA), Italy, and Dipartimento di Fisica "E. R. Caianiello," Università di Salerno, IT-84084 Fisciano (SA), Italy

(Received 19 September 2016; revised manuscript received 28 January 2017; published 6 April 2017)

We investigate the nature of the electronic states in a variety of nonsymmorphic collinear antiferromagnets with glide reflection symmetry, a combination of mirror and half-lattice translation. In particular, the study refers to a class of systems with two-band itinerant electrons that are spin-orbit coupled and interacting with a magnetic background having a zigzag pattern. We describe the symmetry properties of the model system by focusing on the role of nonsymmorphic transformations arising from the antiferromagnetic structure of the spin ordering. Gapless phases with Dirac points having different types of symmetry-protection as well as electronic structures with triple and quadruple band-crossing points are obtained. A glide semimetal is shown to be converted into a gapless phase with Dirac points protected by inversion and time-inversion symmetry combination. Interestingly, we find a relation between the states in the glide sectors that provides a general mechanism to get multiple band touching points. The split of the multiple Fermi points drives the transition from a point node to a line node semimetal or to a metal with nontrivial winding around the Fermi pockets and an electronic structure that is tied to the presence of glide symmetric Dirac points. Besides a new perspective of ordered states in complex materials, our findings indicate relevant paths to topological gapless phases and edge states in a wide class of magnetic systems.

DOI: 10.1103/PhysRevB.95.155108

I. INTRODUCTION

Topological materials have become the focus of intense research in the last years [1–4] not only for the perspective of new physical phenomena with potential technological applications, but also for being a test bed for fundamental concepts of physics theories. Along this line, recent efforts led to the theoretical prediction [5–8] and experimental realization [9–11] of topological insulators in materials with strong spin-orbit coupling (SOC). One of the hallmarks of TIs is the existence of protected gapless edge states, which are due to a nontrivial topology of the bulk band structure. Such manifestation of topological order, however, is not limited to insulators as electronic structures with gapless topological modes have been predicted [12–20] and their relevance further boosted by the discovery of novel materials [21–23,30–32] with nontrivial band crossing points in the momentum space and robust edge states.

Among various kinds of topological matter, correlated materials [24,25] with strong spin-orbital-charge entanglement [26–29], e.g., transition-metal oxides, represent a unique platform to explore topological effects combined to a large variety of intriguing collective properties emerging from electron-electron interaction, as superconductivity, magnetism, magnetoelectricity and Mott insulating phases. In these systems, complex magnetic orders generally arise from competing ferromagnetic (FM) and antiferromagnetic (AF) correlations with a frustrated localized-itinerant nature and a strong dependence on the orbital character of the transition metal d shells. Magnetic patterns constructed by antiferromagnetically coupled zigzag FM chains [Figs. 1(a) and 1(b)] are one generic manifestation of such competing effects and often occur in the class of correlated materials as demonstrated in manganites [37–39], ruthenates [40–43], dichalcogenides [44–46], iridates [47,48], nickelates [49–52], etc. A relevant mark of zigzag patterns is the symmetry under nonsymmorphic (NS) transformations that combine point group operations with translation that are a fraction of a Bravais lattice vector [36]. Recently, NS groups have been recognized as a new source of topological symmetry protection both in gapped [53–66] and gapless [67–81] systems. Hence, given the wide range of physical phenomena in both topological and correlated materials, the identification of novel topological phases in the presence of nontrivial orderings and their material realizations represent a fundamental challenge in the condensed matter area.

In this paper, we investigate the nature of the electronic states occurring in a variety of nonsymmorphic collinear antiferromagnets with glide reflection symmetry. In particular, the study refers to a class of systems with two-orbital itinerant electrons that are coupled to an antiferromagnetic background having a zigzag pattern (Fig. 1). We describe the symmetry properties of the model Hamiltonian by focusing on the role of nonsymmorphic transformations that arise from the antiferromagnetic structure of the spin ordering. The electronic phase diagram reflects the rich symmetry structure of the model system. It exhibits different types of insulating configurations that are separated or surrounded in the parameters space by a variety of gapless states with distinct symmetry protection and topological features. Indeed, we find semimetal (SM) phases with Dirac points (DPs) exhibiting different type of symmetry protection as well as three- and fourfold degeneracy. Besides the nonsymmorphic glide symmetry protection, we demonstrate that combination of inversion and time or particle-hole symmetry can also protect the DPs, thus building up robust gapless phases. Remarkably, we find a relation between the states in the two glide sectors that explains the origin of the multiple band touching points in the glide plane and provides a general mechanism for sticking the DPs. We show that the splitting of multiple degenerate Fermi points (FPs) leads to anomalous gapless phases. Indeed, due to the symmetry protection of the DPs in the glide plane and the presence of a chiral nonsymmorphic symmetry, a transition from a point node semimetal to a gapless phase with a line of semi-Dirac points can be obtained. Otherwise, close to the

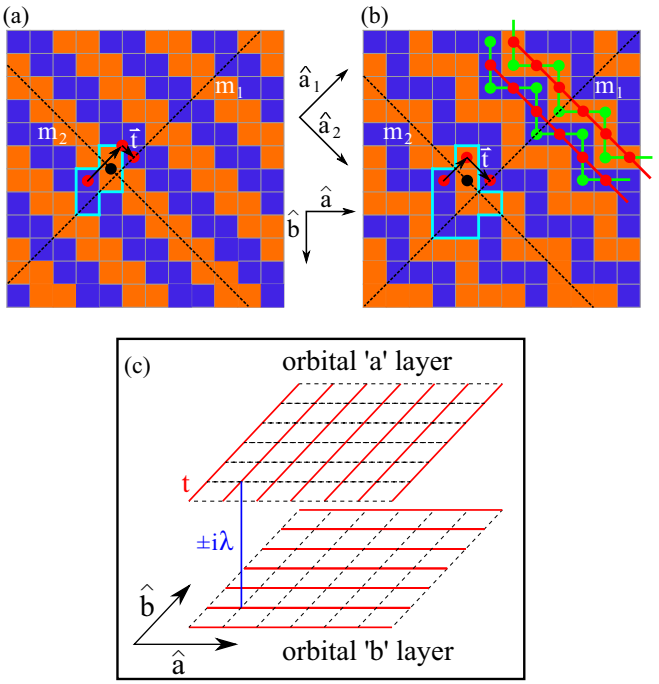

FIG. 1. Zigzag spin patterns with (a) length $L_z = 2$ ($z2$), (b) $L_z = 3$ ($z3$), and (c) schematic view of the orbital dependent hopping processes in undistorted system—orbital flavors a/b can be associated to effective layers of a single-band bilayer system. In this framework, the spin-orbit coupling λ acts as an interlayer antisymmetric hopping. Orange and blue squares indicate spin-up and spin-down orientation. The unit cell is marked by a thick blue frame while $\hat{a}_{1,2}$ are the translation directions. Dashed lines indicate the mirror planes m_1 and m_2, with m_2 being related to the gliding symmetry. The effect of the glide transformation is sketched by the red dots and the black arrows; the dot is subjected to the reflection m_2 then it is translated by a vector $\vec{t}$ parallel to the mirror plane m_2. For the $z2$ configuration, these two steps separately do not reproduce the original lattice. For the $z3$ phase, the connected red and green dots indicate the additional second and third neighbor hopping processes that preserve all the symmetries of the Hamiltonian. The black dots are the inversion centers.

triple band-touching point the electronic structure is marked by multiple Fermi pockets with nontrivial winding number.

The paper is organized as follows. In Sec. II, we present the model Hamiltonian employed to describe the zigzag antiferromagnets. The symmetry properties of the model system are provided in Sec III. Section IV is devoted to the phase diagram and the analysis of the most relevant gapless configurations emerging among the obtained electronic structures. In Sec. V, we provide the summary and the concluding remarks. Other details related with the symmetries of the Hamiltonian and the zigzag antiferromagnetic phases are given in the Appendices A–D.

II. MODEL

We consider an effective orbital-directional double-exchange model describing itinerant electrons (e.g., t_{2g} or p bands) in the presence of an anisotropic SOC, as due to tetragonal crystal field splitting, and Hund coupled to localized spin moments forming zigzag pattern with characteristic length $L_z \geqslant 2$. The model Hamiltonian is given by

$$\mathcal{H} = \sum_{i,\sigma} \sum_{\substack{\alpha,\beta=a,b \\ \hat{\gamma}=\hat{a},\hat{b}}} -t_{\gamma,\alpha\beta}(d^{\dagger}_{i,\alpha\sigma} d_{i+\hat{\gamma},\beta\sigma} + \text{H.c.}) - J_H \sum_{i,\alpha=a,b} s^z_{i\alpha} \cdot S^z_i + \lambda \sum_i S^z_i l^z_i \,, \tag{1}$$

where $d^{\dagger}_{i,\alpha\sigma}$ is the electron creation operator at the site i with spin σ for the orbital α, (a,b,c) are the (yz,xz,xy) orbitals, which are perpendicular to the corresponding bond direction, with $\hat{a}$, $\hat{b}$, and $\hat{c}$ being the unit vectors along the lattice symmetry directions. α, $\mathbf{s}_{i\alpha} = d^{\dagger}_{i,\mu,\alpha}\sigma^z_{\alpha,\beta} d_{i,\mu,\beta}$ and $S^z_i = \pm 1$ denote the spins for the $d_{xz/yz}$ and d_{xy} orbitals, respectively. J_H stands for the Hund coupling, while λ is the SOC for the projected subspace of (a,b) orbitals, with $l^z_i = i(d^{\dagger}_{i,a,\sigma} d_{i,b,\sigma} - d^{\dagger}_{i,b,\sigma} d_{i,a,\sigma})$ the z component of the local angular momentum. $t_{\hat{\gamma},\alpha\beta}$ is the nearest-neighbor hopping amplitude between α and β for the bond along the $\hat{\gamma}$ direction. We assume tetragonal symmetric hopping amplitudes, i.e., $t_{\hat{a},bb} = t_{\hat{b},aa} = t$ with t as energy scale unit and $t_{\hat{\gamma},ab} = 0$—see Fig. 1(c) for the schematic view of the hopping processes. The AF states are collinear and the spin z projection is a conserved quantity due to the anisotropic SOC.

While the Hamiltonian resembles the double-exchange model widely applied in the context of manganese oxides, it contains extra microscopic ingredients as orbital directionality and spin-orbit coupling that contribute to give unique features in the phase diagram and the electronic spectra. For instance, zigzag states have been demonstrated to be among the energetically most favorable configurations in a large range of doping concentration for the case of $d_{xz/yz}$ bands [33] and orbital directionality is a key ingredient for understanding the occurrence of zigzag spin patterns with length $L_z = 2$ (i.e., $z2$) in Mn-doped bilayer ruthenates $Sr_3Ru_2O_7$ and in other similar hybrid oxides. Furthermore, the model Hamiltonian has a more general range of application as it can be considered as an effective low-energy description of correlated t_{2g} electrons in transition metal oxides with orbital selective localized and itinerant bands such as to yield a double exchange model. Indeed, as a consequence of the atomic Coulomb interaction in multiorbital systems, an orbital selective Mott transition can occur and lead to electronic localization in a subgroup of the t_{2g} bands. Such reduction from a multiorbital correlated system to an effective double exchange has been generally addressed and demonstrated to be applicable in the context of orbital-selective Mott physics [34,35].

The general form of the Hamiltonian in Eq. (1) for a zigzag spin pattern can be obtained by analyzing the possible hopping processes for a given unit cell, as shown in Fig. 1. Its matrix representation for a given momentum $\vec{k}$ and fixed spin polarization of the itinerant electrons, being a good quantum number, can be conveniently written as a block matrix in the form

$$\mathcal{H}_{\vec{k}} = \begin{pmatrix} \mathbf{H}^{bb}_{\downarrow\downarrow} & \mathbf{H}^{bb}_{\downarrow\uparrow} & \mathbf{H}^{ba}_{\downarrow\downarrow} & \mathbf{H}^{ba}_{\downarrow\uparrow} \\ \mathbf{H}^{bb}_{\uparrow\downarrow} & \mathbf{H}^{bb}_{\uparrow\uparrow} & \mathbf{H}^{ba}_{\uparrow\downarrow} & \mathbf{H}^{ba}_{\uparrow\uparrow} \\ \mathbf{H}^{ab}_{\downarrow\downarrow} & \mathbf{H}^{ab}_{\downarrow\uparrow} & \mathbf{H}^{aa}_{\downarrow\downarrow} & \mathbf{H}^{aa}_{\downarrow\uparrow} \\ \mathbf{H}^{ab}_{\uparrow\downarrow} & \mathbf{H}^{ab}_{\uparrow\uparrow} & \mathbf{H}^{aa}_{\uparrow\downarrow} & \mathbf{H}^{aa}_{\uparrow\uparrow} \end{pmatrix}. \tag{2}$$

Here, the blocks $\mathbf{H}^{\alpha\beta}_{\sigma\sigma'}(\sigma,\sigma'=\uparrow,\downarrow$ and $\alpha,\alpha'=a,b)$ are of size $N_\downarrow = N_\uparrow = 2L_z - 2$, associated to the spin-up and spin-down domains within the unit cell (see Fig. 1). The indices $(\sigma\alpha)$ and $(\sigma'\beta)$ mean that the block describes hopping processes from the spin σ to spin σ' domains and orbitals α and β, respectively. For instance, for $z2$ magnetic pattern, the blocks for the electrons in the b-orbital sector are given by the equations

$$\mathbf{H}^{bb}_{\sigma\sigma} = \begin{pmatrix} -\sigma J_H & -e^{-ik_2}t \\ -e^{ik_2}t & -\sigma J_H \end{pmatrix}, \quad \mathbf{H}^{bb}_{\downarrow\uparrow} = (\mathbf{H}^{bb}_{\uparrow\downarrow})^\dagger = \begin{pmatrix} 0 & -t \\ -e^{-ik_1}t & 0 \end{pmatrix}, \tag{3}$$

while for the a-orbital sector are

$$\mathbf{H}^{aa}_{\sigma\sigma} = \begin{pmatrix} -\sigma J_H & -t \\ -t & -\sigma J_H \end{pmatrix}, \quad \mathbf{H}^{aa}_{\downarrow\uparrow} = \left(\mathbf{H}^{aa}_{\uparrow\downarrow}\right)^\dagger = \begin{pmatrix} 0 & -e^{-ik_2}t \\ -e^{i(k_2-k_1)}t & 0 \end{pmatrix}. \tag{4}$$

Concerning the interorbital sector, the only nonvanishing entries in the undistorted system are those which originate from SOC, i.e.,

$$\mathbf{H}^{ba}_{\sigma\sigma} = \left(\mathbf{H}^{ab}_{\sigma\sigma}\right)^\dagger = -i\sigma\lambda\mathbf{1}, \quad \mathbf{H}^{ba}_{\sigma,-\sigma} = \left(\mathbf{H}^{ab}_{\sigma,-\sigma}\right)^\dagger = \mathbf{0}. \tag{5}$$

We note that the spin sectors for the itinerant electrons are completely equivalent. For the zigzag $z3$, the size of the spin domain is $N_\downarrow = 4$ and thus the blocks are twice larger. Then, for the b-orbital sector, we have

$$\mathbf{H}^{bb}_{\sigma\sigma} = \begin{pmatrix} -\sigma J_H & 0 & 0 & -e^{-ik_2}t \\ 0 & -\sigma J_H & 0 & 0 \\ 0 & 0 & -\sigma J_H & -t \\ -e^{ik_2}t & 0 & -t & -\sigma J_H \end{pmatrix}, \quad \mathbf{H}^{bb}_{\downarrow\uparrow} = (\mathbf{H}^{bb}_{\uparrow\downarrow})^\dagger = \begin{pmatrix} 0 & -t & 0 & 0 \\ -e^{-ik_1}t & 0 & -t & 0 \\ 0 & -e^{-ik_1}t & 0 & 0 \\ 0 & 0 & 0 & 0 \end{pmatrix}, \tag{6}$$

and for the a-orbital sector

$$\mathbf{H}^{aa}_{\sigma\sigma} = \begin{pmatrix} -\sigma J_H & -t & 0 & 0 \\ -t & -\sigma J_H & -t & 0 \\ 0 & -t & -\sigma J_H & 0 \\ 0 & 0 & 0 & -\sigma J_H \end{pmatrix}, \quad \mathbf{H}^{aa}_{\downarrow\uparrow} = (\mathbf{H}^{aa}_{\uparrow\downarrow})^\dagger = \begin{pmatrix} 0 & 0 & 0 & -e^{-ik_2}t \\ 0 & 0 & 0 & 0 \\ 0 & 0 & 0 & -e^{-ik_1}t \\ -e^{i(k_2-k_1)}t & 0 & -t & 0 \end{pmatrix}. \tag{7}$$

The structure of the mixing orbitals sector is the same as in Eq. (5).

When dealing with zigzag $z3$, we are also interested in long-range hopping processes as they will be relevant for analyzing the evolution of the electronic structure upon the application of symmetry conserving perturbations. These are second- and third-neighbor hoppings along the zigzag paths that connect corresponding corners and internal sites within the vertical and horizontal three-site segments [see Fig. 1 (b)]. A distinct feature of such terms is that they preserve all the symmetries of the Hamiltonian (1) as we will discuss thoroughly in the next section. In presence of these hopping processes with amplitude δ the intraorbital-intradomain blocks $\mathbf{H}^{\alpha\alpha}_{\sigma\sigma}$ are modified in the following way, $\mathbf{H}^{\alpha\alpha}_{\sigma\sigma} \to \mathbf{H}^{\alpha\alpha}_{\sigma\sigma} + \mathbf{h}^{\alpha\alpha}_{\sigma\sigma}$ with

$$\mathbf{h}^{\alpha\alpha}_{\sigma\sigma} = \delta\sigma \begin{pmatrix} 0 & 0 & 1+e^{-ik_2} & 0 \\ 0 & 0 & 0 & 1+e^{-ik_2} \\ 1+e^{ik_2} & 0 & 0 & 0 \\ 0 & 1+e^{ik_2} & 0 & 0 \end{pmatrix}. \tag{8}$$

III. SYMMETRIES

The symmetry properties of the model Hamiltonian include transformations that act on the internal (e.g., spin, orbital, charge) and spatial degrees of freedom, or combine them, including the possibility of having groups with fractional nonprimitive lattice vector translational (i.e., nonsymmorphic groups). In this section, we will present the structure and properties of the internal, symmorphic, and nonsymmorphic symmetries exhibited by the model Hamiltonian in Eq. (1). Furthermore, we will provide both the explicit expressions of the symmetry operators and the relevant aspects of their structure. We focus on the fundamental marks and consequences that are related to the presence of nonsymmorphic glide transformations and in general to nonsymmorphic symmetries arising from the antiferromagnetic spin pattern.

A. Internal symmetries

Concerning the internal symmetries, the model exhibits time reversal invariance. Indeed, the electrons are coupled to a magnetic background with a collinear order, thus the localized spins can be treated as classical variables and, consequently, there is no mixing between the spin up and down sectors for the itinerant electrons, with their spin orientation being a good quantum number. Then, the time-reversal operation can be constructed by combining complex conjugation and a unitary transformation $\mathcal{T}$ that satisfies the ordinary relation

$$\mathcal{T}^\dagger \mathcal{H}_{\vec{k}} \mathcal{T} = \mathcal{H}^T_{-\vec{k}}. \tag{9}$$

The transposition on the right-hand side is equivalent to complex conjugation, so that the whole transformation is

antiunitary. Within a given block of $\mathcal{H}_{\vec{k}}$ for the $z2$ and $z3$ zigzag patterns, the complex conjugation acts by changing all the $\vec{k}$ to $-\vec{k}$ and makes λ to become $-\lambda$. We can employ the correspondence of the two orbital flavors with two independent effective layers of the square lattice [Fig. 1(c)] to directly deduce that, in the absence of interorbital hopping, i.e, when no distortions are present, the change of sign in λ can be absorbed by a gauge transformation of the form

$$\begin{aligned} d^{(\dagger)}_{i,a,\sigma} &= -\tilde{d}^{(\dagger)}_{i,a,\sigma}, \\ d^{(\dagger)}_{i,b,\sigma} &= \tilde{d}^{(\dagger)}_{i,b,\sigma}, \end{aligned} \tag{10}$$

where $\tilde{d}^{(\dagger)}$ are the transformed fermion operators. Since for the orbital directional model all the hopping processes are orbital-conserving, i.e., there is no effective interorbital mixing, the only effect of this gauge transformation is to change the sign of λ. Hence, the form of the operator $\mathcal{T}$ can be expressed as

$$\mathcal{T} = \begin{pmatrix} \mathbf{1}^b_\downarrow & \mathbf{0} & \mathbf{0} & \mathbf{0} \\ \mathbf{0} & \mathbf{1}^b_\uparrow & \mathbf{0} & \mathbf{0} \\ \mathbf{0} & \mathbf{0} & -\mathbf{1}^a_\downarrow & \mathbf{0} \\ \mathbf{0} & \mathbf{0} & \mathbf{0} & -\mathbf{1}^a_\uparrow \end{pmatrix}, \tag{11}$$

where $\mathbf{1}$ denotes a unit matrix of the size $N_\downarrow$ and the indices indicate the spin/orbital sectors, respectively. Furthermore, the matrix is purely real and thus we have that $\mathcal{T}^2 = 1$.

B. Spatial symmetries

For the clarity of the presentation and for the discussion of the resulting electronic spectra, concerning the spatial symmetries it is useful to distinguish between the operations that are symmorphic (i.e., related to the point group) from those that are nonsymmorphic because they involve a translation of half of the primitive lattice vector. Indeed, as already pointed out in the introduction, the system upon examination deals with itinerant electrons in a square lattice coupled to an underlying magnetic background of localized spins with a zigzag pattern. Specific of the zigzag magnetic patterns is the invariance under a nonsymmorphic (NS) glide transformation $\mathcal{R}^t$ which is constructed by the product of a mirror transformation with respect to the m_2 line and a translation $\vec{t} \equiv \vec{a}_2/2$ in the $\hat{a}_2$ direction along the zigzag chain as demonstrated in the Figs. 1(a) and 1(b). Such relation is consistent with the expectation in two dimensions of other relevant symmetry operations than those of the crystal point group, belonging to the nonsymmorphic groups which may include screw axis, glide mirror lines, and glide mirror planes in conjunction with the translation [36].

1. Mirror reflection

Concerning the symmorphic symmetries, we observe that the system is invariant under a mirror transformation with respect to the reflection line m_1. The reflection line for a zigzag pattern with size $L_z = 2$ and 3 is explicitly shown in Figs. 1(a) and 1(b) and can be easily generalized for any L_z. Its direction is diagonal with respect to the symmetry axes, thus it acts by interchanging the hoppings along the a and b directions. Such transformation, then, requires an exchange of the orbitals a and b to preserve the connectivity of the system before performing the reflection. Furthermore, since the sign of λ is also modified by the orbital exchange, one can employ again a gauge transformation, as given by Eq. (10), to build up the symmetry conserving transformation. An alternative way to visualize the action of the mirror is to employ the correspondence of the two-dimensional (2D) system with two orbital flavors with an effective single-band bilayer, as schematically depicted in Fig. 1(c). In this framework, the reflection can be understood as a π-rotation with respect to the axis parallel to the reflection line m_1. Such operation naturally interchanges the layers and thus the orbital flavors. Since the selected elementary cell of the zigzag system shown in Figs. 1(a) and 1(b) is not invariant upon the application of the mirror transformation, the reflection operator depends on the momentum k_2 and has the form

$$\mathcal{R}_{k_2} = \begin{pmatrix} \mathbf{0} & \mathbf{0} & \mathbf{R}_{k_2} & \mathbf{0} \\ \mathbf{0} & \mathbf{0} & \mathbf{0} & \mathbf{R}_{k_2} \\ -\mathbf{R}_{k_2} & \mathbf{0} & \mathbf{0} & \mathbf{0} \\ \mathbf{0} & -\mathbf{R}_{k_2} & \mathbf{0} & \mathbf{0} \end{pmatrix}, \tag{12}$$

with blocks of size $N_\downarrow \times N_\downarrow$ given by

$$\mathbf{R}_{k_2} = \begin{pmatrix} i & 0 & 0 & \cdots & 0 & 0 \\ 0 & 0 & 0 & \cdots & 0 & ie^{ik_2} \\ 0 & 0 & 0 & \cdots & ie^{ik_2} & 0 \\ 0 & 0 & ie^{ik_2} & \cdots & 0 & 0 \\ 0 & ie^{ik_2} & 0 & \cdots & 0 & 0 \end{pmatrix}. \tag{13}$$

The $\mathbf{R}_{k_2}$ is a unitary operator satisfying the following relation with the Hamiltonian

$$\mathcal{R}^\dagger_{k_2} \mathcal{H}_{k_1,k_2} \mathcal{R}_{k_2} = \mathcal{H}_{k_1,-k_2}. \tag{14}$$

Despite the dependence on k_2 the eigenvectors of $\mathcal{R}_{k_2}$ can be constructed as not depending on k_2 and its diagonal form is given by the equation,

$$\mathcal{U}^\dagger \mathcal{R}_{k_2} \mathcal{U} = \begin{pmatrix} \mathbf{1}_2 & \mathbf{0} & \mathbf{0} & \mathbf{0} \\ \mathbf{0} & e^{ik_2}\mathbf{1}_{2N_\downarrow - 2} & \mathbf{0} & \mathbf{0} \\ \mathbf{0} & \mathbf{0} & -\mathbf{1}_2 & \mathbf{0} \\ \mathbf{0} & \mathbf{0} & \mathbf{0} & -e^{ik_2}\mathbf{1}_{2N_\downarrow - 2} \end{pmatrix}, \tag{15}$$

where $\mathcal{U}$ is the eigenbasis and the blocks are unity matrices of size 2 or $2N_\downarrow - 2$. We note that for any zigzag segment length there are two eigenvalues of amplitude 2, and other two with value -2 while the remaining part of the spectrum is given by $\pm e^{ik_2}$. The spectrum is chiral in the sense that for any eigenvalue there is a partner with opposite sign. Furthermore, in the reflection planes at $k_2 = 0,\pi$ the reflection operator becomes a symmetry for the Hamiltonian, i.e.,

$$\left[\mathcal{H}_{k_1,0(\pi)}, \mathcal{R}_{0(\pi)}\right] = 0 \tag{16}$$

and there is no k dependence in the spectrum of $\mathcal{R}_{k_2}$, being equal to $+1$ at $k_2 = 0$ and -1 at $k_2 = \pi$. Consistently with its symmorphic character, the reflection operator $\mathcal{R}$ can be made completely k-independent by choosing a unit cell that maps

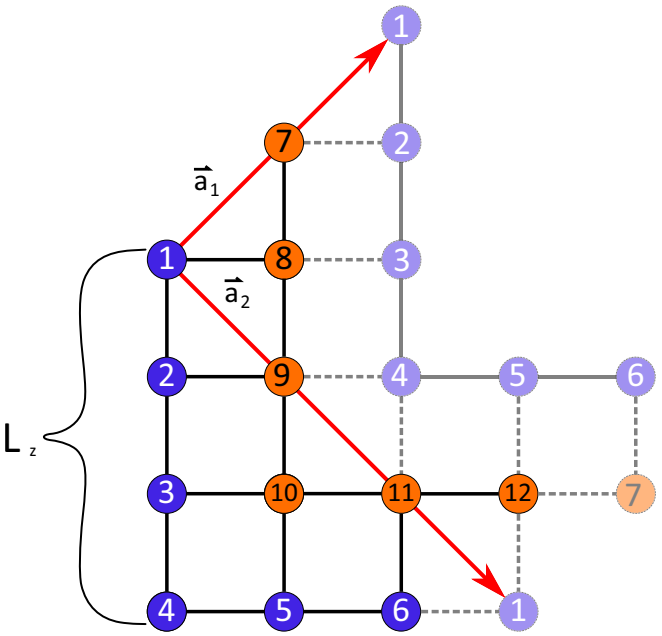

FIG. 2. Schematic view of the unit cell for zigzag of exemplary length of $L_z = 4$ and labeling of the intracell sites for one orbital flavor. Orange and blue circles indicate the sites with spin up and down, respectively. The number of sites in the magnetic domain is $N_\downarrow = 2L_z - 2 = 6$. Solid lines connect sites belonging to one unit cell whereas the dashed lines connect sites of neighboring unit cells. The primitive lattice translation vectors $\vec{a}_{1,2}$ are shown explicitly.

onto itself under the reflection or, equivalently, by a suitable gauge transformation (see Appendix B for details).

2. Nonsymmorphic chirality

An important aspect related to the intrinsic antiferromagnetic structure of the zigzag pattern is that the Hamiltonian in Eq. (1) has a sublattice or chiral symmetry that exhibits a nonsymmorphic structure. Indeed, one can find a unitary operator $\mathcal{S}_{k_1}$ that anticommutes with Hamiltonian and is explicitly momentum dependent as

$$\mathcal{S}_{k_1}^\dagger \mathcal{H}_{\vec{k}} \mathcal{S}_{k_1} = -\mathcal{H}_{\vec{k}}\,. \tag{17}$$

For the problem upon examination, such symmetry occurs only at half-filling and arises from the two sublattice structure of the two magnetic domains within a unit cell as indicated by different colors in Fig. 2. By inspection of the Fig. 2, one can observe that in order to move from one to another domain, a translation $\vec{a}_1/2$ is needed. For this reason, the operator S_{k_1} depends on the momentum k_1 and has nonzero blocks that connect opposite spin domains within the same orbital sectors, i.e.,

$$\mathcal{S}_{k_1} = \begin{pmatrix} \mathbf{0} & \mathbf{S}_{k_1} & \mathbf{0} & \mathbf{0} \\ \mathbf{S}_{k_1}^\dagger & \mathbf{0} & \mathbf{0} & \mathbf{0} \\ \mathbf{0} & \mathbf{0} & \mathbf{0} & \mathbf{S}_{k_1} \\ \mathbf{0} & \mathbf{0} & \mathbf{S}_{k_1}^\dagger & \mathbf{0} \end{pmatrix}, \tag{18}$$

with

$$\mathbf{S}_{k_1} = e^{-i\frac{k_1}{2}} \begin{pmatrix} -1 & 0 & 0 & \cdots & 0 \\ 0 & 1 & 0 & \cdots & 0 \\ 0 & 0 & -1 & \cdots & 0 \\ \vdots & \vdots & \vdots & \ddots & 0 \\ 0 & 0 & 0 & 0 & 1 \end{pmatrix}. \tag{19}$$

Apart from the change of the spin-domain there is a phase factor of $e^{-i\frac{k_1}{2}}$ appearing with alternating sign $(-1)^i$ as one moves along the zigzag segment (i.e., from site $i = 1$ to $i = 8$ in Fig. 2). The alternation is related to the change of the sign for the allowed hoppings along the bonds of the square lattice. Here, the chiral symmetry arises because the zigzag sublattice structure of the magnetic domains is compatible with the natural two-sublattice structure of the square lattice.

In order to better specify the character of the nonsymmorphic transformation and to make more direct the connection with the available tables of topological classifications of fully gapped states with nonsymmorphic symmetry [56], it is useful to introduce the notion of flipped coordinates $d_\parallel$ as done in Ref. [56]. Indeed, $d_\parallel$ indicates the number of components of $\vec{k}$ that change sign under the action of a given nonsymmorphic transformation. In this context, $\mathcal{S}_{k_1}$ is an order-two nonsymmorphic operator with $d_\parallel = 0$. Taking into account the classification of fully gapped electronic states of Ref. [56], such type of symmetry is expected to lead to topologically nontrivial insulating states only in one-dimension for a symmetry class with $\mathcal{T}^2 = 1$. Hence, we observe that for our 2D system the fully gapped phases are expected to be topologically trivial.

3. Nonsymmorphic glide mirror reflection

A relevant spatial symmetry of the class of investigated magnetic configurations is that arising from the nonsymmorphic glide transformation. The glide operation is obtained by the product of a reflection with respect to the line m_2, perpendicular to that one involved in $\mathcal{R}_{k_2}$, and a translation $\vec{t}$ along a direction parallel to the reflection line. One can show that for any zigzag segment length, the translation vector is always given by $\vec{t} = \frac{1}{2}\vec{a}_2$. The action of the glide operation is explicitly shown in Figs. 1(a) and 1(b). We observe that for any zigzag with even L_z both the reflection and translation of the nonprimitive lattice vector do not generally map the original square lattice into itself, but only their product does it. Similarly to the mirror reflection $\mathcal{R}$, the glide symmetry can be represented through a unitary matrix that is mixing the a and b orbitals with the following block structure:

$$\mathcal{R}_{\vec{k}}^t = \begin{pmatrix} \mathbf{0} & \mathbf{0} & -\mathbf{R}_{\vec{k}}^{\mathbf{t}} & \mathbf{0} \\ \mathbf{0} & \mathbf{0} & \mathbf{0} & -e^{ik}\mathbf{R}_{\vec{k}}^{\mathbf{t}} \\ \mathbf{R}_{\vec{k}}^{\mathbf{t}} & \mathbf{0} & \mathbf{0} & \mathbf{0} \\ \mathbf{0} & e^{ik}\mathbf{R}_{\vec{k}}^{\mathbf{t}} & \mathbf{0} & \mathbf{0} \end{pmatrix}, \tag{20}$$

and in turn the given blocks are expressed by matrices of size $L_z - 1 \equiv N_\downarrow/2$ as

$$\mathbf{R}^{\mathbf{t}}_{\vec{k}} = \begin{pmatrix} \mathbf{0} & ie^{-i\frac{k_2}{2}}\mathbf{1}_{L_z-1} \\ ie^{i\frac{k_2}{2}}\mathbf{1}_{L_z-1} & \mathbf{0} \end{pmatrix}. \tag{21}$$

It is useful to employ the correspondence with the bilayer representation to explicitly visualize the effect of the transformation on the spatial and orbital degrees of freedom. Indeed, the glide operation acts as a π rotation with a shift parallel to its axis along the mirror line m_2. $\mathcal{R}^t_{\vec{k}}$ carries the intrinsic dependence on both momenta as a direct consequence of its nonsymmorphic nature. On a general ground, one cannot find a unit cell that maps onto itself under such an operation. The relation with the Hamiltonian is the same as that one for a normal mirror mapping k_1 into $-k_1$, i.e.,

$$\mathcal{R}^{t\dagger}_{\vec{k}}\mathcal{H}_{k_1,k_2}\mathcal{R}^t_{\vec{k}} = \mathcal{H}_{-k_1,k_2}. \tag{22}$$

Concerning the spectral aspects of the glide operator, $\mathcal{R}^t_{\vec{k}}$ has eigenvectors that depend only on k_2 and eigenvalues that depend only on k_1, thus its diagonal form can be expressed by the equation

$$\mathcal{V}^\dagger_{k_2}\mathcal{R}^t_{\vec{k}}\mathcal{V}_{k_2} = \begin{pmatrix} \mathbf{1}_{\mathbf{N}_\downarrow} & \mathbf{0} & \mathbf{0} & \mathbf{0} \\ \mathbf{0} & e^{ik_1}\mathbf{1}_{N_\downarrow} & \mathbf{0} & \mathbf{0} \\ \mathbf{0} & \mathbf{0} & -\mathbf{1}_{N_\downarrow} & \mathbf{0} \\ \mathbf{0} & \mathbf{0} & \mathbf{0} & -e^{ik_1}\mathbf{1}_{N_\downarrow} \end{pmatrix}, \tag{23}$$

where $\mathcal{V}_{k_2}$ is the eigenbasis and the blocks are the unity matrices of the size $N_\downarrow$. In the glide planes at $k_1 = 0,\pi$ the glide operator becomes a symmetry of the Hamiltonian, i.e.,

$$\left[\mathcal{H}_{0(\pi),k_2}, \mathcal{R}^t_{0(\pi),k_2}\right] = 0, \tag{24}$$

and the k-dependent eigenvalues change the sign when going from one glide plane to the other. On the other hand in Appendix B, we show that the glide operator $\mathcal{R}^t_{\vec{k}}$ depends intrinsically only on k_2 (due to the shift $\vec{t}$) and the dependence on k_1 can be removed by a proper modification of the unit cell or, equivalently, by a suitable gauge transformation. After this operation the glide eigenvalues become $g = \pm 1$.

At this stage, it is important to mention that the two main nonsymmorphic symmetries, i.e., glide and chirality, satisfy a nontrivial commutation relation that depends on the character of the zigzag patterns. Indeed, $\mathcal{R}^t_{\vec{k}}$ anticommutes or commutes with $\mathcal{S}_{k_1}$ for even or odd L_z, respectively. See Appendix A for the complete list of commutation relations among the various symmetries.

Finally, we note that $\mathcal{R}^t_{\vec{k}}$ is an order-two nonsymmorphic, unitary symmetry with number of flipped coordinates $d_\parallel = 1$. Hence, according to the classification in Ref. [56], it cannot lead to topologically nontrivial insulating state in 2D for time conserving quantum systems with $\mathcal{T}^2 = 1$.

C. Combined symmetries

In order to complete the structure of the symmetry properties of the system we need to observe that other nonsymmorphic transformations can be obtained by combining the glide and/or chiral operator with time or particle-hole.

1. Particle-hole symmetry

Starting from the previously introduced chiral and time-reversal operators, one can construct a nonsymmorphic particle-hole transformation (PHS) associated to an operator $\mathcal{C}$ that is expressed as $\mathcal{C}_{k_1} \equiv \mathcal{S}_{k_1} \cdot \mathcal{T}$. It satisfies a standard relation with the Hamiltonian, i.e.,

$$\mathcal{C}^\dagger_{k_1}\mathcal{H}_{\vec{k}}\mathcal{C}_{k_1} = -\mathcal{H}^T_{-\vec{k}}, \tag{25}$$

and from the properties of $\mathcal{S}$ and $\mathcal{T}$ one can also deduce that $\mathcal{C}^2 = 1$, meaning that its twofold application on the Hamiltonian gives the identity, i.e., $\mathcal{C}_{k_1}\mathcal{C}^\star_{-k_1} \equiv 1$ (where star is complex conjugation). Furthermore, considering its action, we can also notice that $\mathcal{C}_{k_1}$ is a nonsymmorphic, antiunitary chiral symmetry with number of flipped coordinates $d_\parallel = 2$.

2. Inversion

Having two mirror transformations, as given by Eqs. (14) and (22), one can construct an inversion operator $\mathcal{I}_{\vec{k}}$ satisfying the relation

$$\mathcal{I}^\dagger_{\vec{k}}\mathcal{H}_{k_1,k_2}\mathcal{I}_{\vec{k}} = \mathcal{H}_{-k_1,-k_2}. \tag{26}$$

From the Eqs. (14) and (22), we deduce that the inversion operator has the form

$$\mathcal{I}_{\vec{k}} \equiv -e^{-i\frac{k_2}{2}}\mathcal{R}_{k_2}\mathcal{R}^t_{k_1,-k_2}, \tag{27}$$

with the phase factor being introduced only for convenience of representation. We note that the operators in the product are taken at opposite k_2 because by inserting $\mathcal{I}_{\vec{k}}$ into Eq. (26) one has to consider that the first action is on the Hamiltonian with $\mathcal{R}_{k_2}$ which yields $\mathcal{H}_{k_1,-k_2}$. Then, in order to connect $\mathcal{H}_{k_1,-k_2}$ with $\mathcal{H}_{-k_1,-k_2}$ one has to apply the glide operator at the point $(k_1,-k_2)$. Unlike the reflection and glide operators, the inversion does not mix the orbital sectors and its block structure is

$$\mathcal{I}_{\vec{k}} = \begin{pmatrix} \mathbf{I}_{k_2} & \mathbf{0} & \mathbf{0} & \mathbf{0} \\ \mathbf{0} & e^{ik}\mathbf{I}_{k_2} & \mathbf{0} & \mathbf{0} \\ \mathbf{0} & \mathbf{0} & \mathbf{I}_{k_2} & \mathbf{0} \\ \mathbf{0} & \mathbf{0} & \mathbf{0} & e^{ik}\mathbf{I}_{k_2} \end{pmatrix}, \tag{28}$$

with $\mathbf{I}_{k_2}$ defined by the diagonal sub-blocks of size L_z and $L_z - 2$:

$$\mathbf{I}_{k_2} = \begin{pmatrix} \mathbf{P}_{L_z} & \mathbf{0} \\ \mathbf{0} & e^{ik_2}\mathbf{P}_{L_z-2} \end{pmatrix}. \tag{29}$$

These blocks correspond to the vertical and horizontal sections of the spin down/up segment in the unit cell, respectively, namely, the sites $i = 1, 2, 3, 4$ and $i = 5$ and 6 for the $L_z = 4$ unit cell shown in Fig. 2. Finally, $\mathbf{P}_n$ acts as a simple reflection operator for the straight sections of a zigzag pattern and it is expressed by the following $n \times n$ antidiagonal matrix:

$$\mathbf{P}_n = \begin{pmatrix} 0 & 0 & \cdots & 0 & 1 \\ 0 & 0 & \cdots & 1 & 0 \\ 0 & 1 & \cdots & 0 & 0 \\ 1 & 0 & \cdots & 0 & 0 \end{pmatrix}. \tag{30}$$

We notice that the multiplication of a glide with a reflection leads to an ordinary inversion, not a "gliding inversion" or inversion with a shift. Indeed, zigzags with $L_z = 2$ and $L_z = 3$ have inversion centers and they are explicitly shown in Figs. 1(a) and 1(b). The k dependence in $\mathcal{I}_{k_1,k_2}$ arises from the fact that the unit cell does not map onto itself under the inversion and one can check by construction that this aspect holds for any zigzag length L_z. The case of even and odd L_z are qualitatively different because for even L_z the inversion center does not coincide with any lattice site whereas for odd L_z it correspond with a central site in any vertical or horizontal section of the zigzag pattern. For this reason, the spectrum of $\mathcal{I}_{k_1,k_2}$ for zigzags with even segment length L_z is significantly different from that of odd L_z. For the case of even L_z we have a chiral spectrum of the form,

$$\{\{1\}^{L_z},\{-1\}^{L_z},\{e^{ik_1}\}^{L_z},\{-e^{ik_1}\}^{L_z},\{e^{ik_2}\}^{L_z},$$
$$\{-e^{ik_2}\}^{L_z},\{e^{i(k_1+k_2)}\}^{L_z-2},\{-e^{i(k_1+k_2)}\}^{L_z-2}\},$$

where the notation $\{1\}^{L_z}$ means that, e.g., the eigenvalue 1 is L_z-fold. For odd L_z the spectrum has an inequivalent number of positive and negative values, i.e.,

$$\{\{1\}^{L_z+1},\{-1\}^{L_z-1},\{e^{ik_1}\}^{L_z+1},\{-e^{ik_1}\}^{L_z-1},\{e^{ik_2}\}^{L_z-1},$$
$$\{-e^{ik_2}\}^{L_z-3},\{e^{i(k_1+k_2)}\}^{L_z-1},\{-e^{i(k_1+k_2)}\}^{L_z-3}\}.$$

Furthermore, for odd L_z, one can always accommodate the electrons in the inversion centers that coincide with physical sites of the system. Since there are four inversion centers in each unit cell and two orbitals per site, one can obtain eight eigenstates of $\mathcal{I}_{\vec{k}}$ with *positive* eigenvalues, i.e., $\{1,e^{ik_1},e^{ik_2},e^{i(k_1+k_2)}\}$, all of them being double degenerate. This observation explains why there are more *positive* than *negative* eigenvalues for the case of odd L_z. We note that despite the k dependence in the eigenvalues, the eigenvectors of $\mathcal{I}_{\vec{k}}$ turn out to be k-independent for any L_z. Finally, we observe that $\mathcal{I}_{\vec{k}}$ is a nonsymmorphic, unitary symmetry with $d_\parallel = 2$ and does not lead to topologically nontrivial 2D insulating states in the presence of time reversal invariance having $\mathcal{T}^2 = 1$ [56].

3. Conjugation

The combination of time reversal and inversion can be employed to build up a transformation $\mathcal{K}_{\vec{k}}$ that is expressed as

$$\mathcal{K}_{\vec{k}} \equiv \mathcal{I}_{\vec{k}}\mathcal{T}, \tag{31}$$

and whose action on the Hamiltonian is to make it transposed or complex conjugated

$$\mathcal{K}_{\vec{k}}^\dagger \mathcal{H}_{\vec{k}} \mathcal{K}_{\vec{k}} = \mathcal{H}_{\vec{k}}^T. \tag{32}$$

Thus we can generally indicate $\mathcal{K}_{\vec{k}}$ as a *conjugation* operator. Due to its structure and on the property of $\mathcal{I}$ and $\mathcal{T}$, we find that the square of $\mathcal{K}_{\vec{k}}$ gives the identity

$$\mathcal{K}_{\vec{k}}\mathcal{K}_{\vec{k}}^\star \equiv 1\,. \tag{33}$$

The above property has important implication on the Hamiltonian structure as it allows to find a basis for which $\mathcal{H}_{\vec{k}}$ is purely real.

Let us demonstrate such statement. Since $\mathcal{K}_{\vec{k}}$ is unitary, we can have that $\mathcal{K}_{\vec{k}} = \exp(iK_{\vec{k}})$, with $K_{\vec{k}}$ being Hermitian matrix. Hence, if $\mathcal{K}_{\vec{k}}\mathcal{K}_{\vec{k}}^\star \equiv 1$, then $K_{\vec{k}}$ must be also symmetric and real. On this basis, $K_{\vec{k}}$ can be diagonalized by a real unitary transformation and accordingly for $\mathcal{K}_{\vec{k}}$. The eigenvalues of $\mathcal{K}_{\vec{k}}$ are ± 1, hence it can be put in a diagonal form $\mathcal{D}_\mathcal{K}$ by a suitable unitary and real transformation $\mathcal{U}_{\vec{k}}$:

$$\mathcal{D}_\mathcal{K} \equiv \mathcal{U}_{\vec{k}}^\dagger \mathcal{K}_{\vec{k}} \mathcal{U}_{\vec{k}} = \begin{pmatrix} \mathbf{1} & \mathbf{0} \\ \mathbf{0} & -\mathbf{1}\,. \end{pmatrix}. \tag{34}$$

Furthermore, we can introduce another unitary transformation $\mathcal{V}_{\vec{k}}$ as

$$\mathcal{V}_{\vec{k}} \equiv \mathcal{U}_{\vec{k}}\sqrt{\mathcal{D}_\mathcal{K}}, \tag{35}$$

in such a way that the Hamiltonian $\mathcal{H}$ can be transformed into $\mathcal{H}'_{\vec{k}}$

$$\mathcal{H}'_{\vec{k}} = \mathcal{V}_{\vec{k}}^\dagger \mathcal{H}_{\vec{k}} \mathcal{V}_{\vec{k}}. \tag{36}$$

It is then important to observe that the transformed Hamiltonian is purely real. To achieve this result one needs to construct $\mathcal{K}'$ via $\mathcal{V}$, recalling that $\mathcal{K}$ transforms as an antiunitary operator. Indeed, one obtains

$$\mathcal{K}'_{\vec{k}} = \mathcal{V}_{\vec{k}}^T \mathcal{K}_{\vec{k}} \mathcal{V}_{\vec{k}}, \tag{37}$$

and from the definition of $\mathcal{V}_{\vec{k}}$ and from the fact that $\mathcal{U}_{\vec{k}}$, we get

$$\mathcal{K}'_{\vec{k}} = 1. \tag{38}$$

On the other hand, $\mathcal{K}'$ satisfies a relation with $\mathcal{H}'_{\vec{k}}$, which is given by

$$(\mathcal{K}'_{\vec{k}})^\dagger \mathcal{H}'_{\vec{k}} \mathcal{K}'_{\vec{k}} = (\mathcal{H}'_{\vec{k}})^T. \tag{39}$$

Hence, we can finally conclude that $\mathcal{H}'_{\vec{k}} \equiv (\mathcal{H}'_{\vec{k}})^T$ thus implying that $\mathcal{H}'_{\vec{k}}$ is purely real. The occurrence of such a symmetry property represents a constraint for the low-energy structure of the Hamiltonian at any given k point and, as we will discuss in Sec. IV, it can significantly affect the character of the semimetal phases.

As a nonsymmorphic transformation, $\mathcal{K}_{\vec{k}}$ is antiunitary and it does not lead to any sign change of the coordinates, thus $d_\parallel = 0$. In this respect, it is not expected to yield topologically nontrivial 2D insulating states in the presence of time reversal invariance with $\mathcal{T}^2 = 1$ [56].

4. Anticonjugation

Combining the conjugation and the chirality operators we can obtain an *anticonjugation* operator $\mathcal{A}_{\vec{k}}$ that is given by

$$\mathcal{A} \propto \mathcal{S}_{k_1}\mathcal{K}_{\vec{k}}. \tag{40}$$

Its action on the Hamiltonian can be deduced by the relations of the constituent operators, namely

$$\mathcal{A}_{\vec{k}}^\dagger \mathcal{H}_{\vec{k}} \mathcal{A}_{\vec{k}} = -(\mathcal{H}_{\vec{k}})^T. \tag{41}$$

By construction, for zigzag $L_z = 2$, the operator $\mathcal{A}$ turns out to be imaginary whereas for $L_z = 3$ (and any other odd L_z) the anticonjugation operator is purely real. In general, we find that

$$\mathcal{A}_{\vec{k}}\mathcal{A}_{\vec{k}}^\star \equiv (-1)^{L_z+1}\,. \tag{42}$$

Thus, following the same approach described in the previous section, one can demonstrate the existence of a transformation for which the Hamiltonian satisfies the relation $\mathcal{H}'_{\vec{k}} \equiv -(\mathcal{H}'_{\vec{k}})^T$. This means that, for instance, in the case of $L_z = 3$, we can find a basis where the Hamiltonian is purely imaginary while this is not possible for $L_z = 2$. Such difference follows from the commutation rule between inversion (or glide) operator and chirality.

Similarly to $\mathcal{K}_{\vec{k}}$, $\mathcal{A}_{\vec{k}}$ is an antiunitary nonsymmorphic symmetry with $d_{\parallel} = 0$. However, due to the anticommutation relation with $\mathcal{H}_{\vec{k}}$ it represents a chiral symmetry transformation.

5. Time reversal in the one-dimensional cuts of the Brillouin zone

Due to the presence of the time-reversal operator $\mathcal{T}$ together with two reflection symmetries (one of which is the glide mirror), one can construct operators which behave like effective time reversal transformations in the one-dimensional (1D) cuts of the Brillouin zone (BZ) for any cut at given k_1 and k_2. An interesting observation is that, though the 2D time-reversal operator fulfills the relation $\mathcal{T}^2 = 1$, the lower dimensional time reversal transformations can have different properties. Hence, in principle, the electronic spectra can be in a different Altland-Zirnbauer class in the projected 1D cuts of the BZ when compared to the whole 2D system.

We start by considering the combination of time and reflection that yields the symmetry operator $\mathcal{T}^{(1)}_{k_2}$ expressed as

$$\mathcal{T}^{(1)}_{k_2} \equiv \mathcal{R}_{k_2}\mathcal{T}\,. \tag{43}$$

$\mathcal{T}_{k_2}$ acts in the 1D cuts of BZ, which are parallel to the k_1 axis (k_1 cuts) in such a way that

$$\mathcal{T}^{(1)\dagger}_{k_2}\mathcal{H}_{k_1,k_2}\mathcal{T}^{(1)}_{k_2} = \mathcal{H}^{T}_{-k_1,k_2}. \tag{44}$$

In the same way, for the glide symmetry, we can introduce the operator $\mathcal{T}^{(2)}_{k_1,k_2}$, which is given by

$$\mathcal{T}^{(2)}_{k_1,k_2} \equiv \mathcal{R}^{t}_{k_1,k_2}\mathcal{T}, \tag{45}$$

and acts along the cuts parallel to the k_2 axis (k_2 cuts) such as

$$\mathcal{T}^{(2)\dagger}_{k_1,k_2}\mathcal{H}_{k_1,k_2}\mathcal{T}^{(2)}_{k_1,k_2} = \mathcal{H}^{T}_{k_1,-k_2}. \tag{46}$$

A close inspection of these two antiunitary symmetries shows that for the k_1 cuts in the BZ the time reversal squares to one, i.e.,

$$\mathcal{T}^{(1)}_{k_2}\mathcal{T}^{(1)\star}_{k_2} \equiv 1, \tag{47}$$

whereas for the k_2 cuts we have a k-dependent result,

$$\mathcal{T}^{(2)}_{k_1,k_2}\mathcal{T}^{(2)\star}_{k_1,-k_2} \equiv e^{-ik_2}. \tag{48}$$

This means that at the two time-reversal points of a given k_2 cut, i.e., at $k_2 = 0$ and $k_2 = \pi$, we have $(\mathcal{T}^{(2)})^2 = 1$ and $(\mathcal{T}^{(2)})^2 = -1$, respectively. Then, one can conclude that for any k_2-cut the point $k_2 = \pi$ is twofold Kramers degenerate. The direct consequence on the electronic structure is that for any L_z the system at $k_2 = \pi$ exhibits a line of double degenerate points as a function of k_1. In Fig. 3, we explicitly demonstrate the presence of the Kramers degenerate points at $k_2 = \pi$ for both the case of $L_z = 2$ and $L_z = 3$ zigzag configurations.

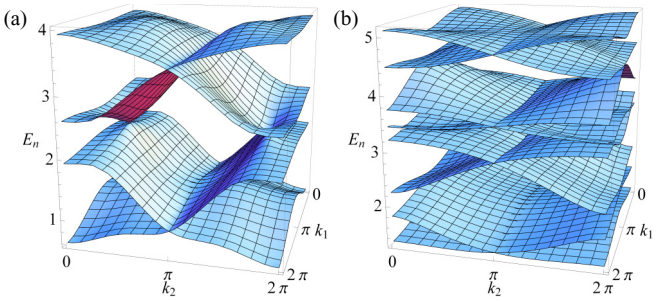

FIG. 3. Positive-energy bands of the undistorted tetragonal zigzag systems: (a) $L_z = 2$ and (b) 3. The negative-energy bands can be recovered by reflection with respect to zero energy due to the chirality $\mathcal{S}_{k_1}$. We note that the bands appear in $(2L_z - 2)$ pairs and every pair has a 1D crossing line at $k_2 = \pi$ due to the occurrence of an effective Kramers degeneracy at any cut along k_2 direction. These pairs are Kramers doublets at $k_2 = \pi$.

6. Symmetry in the parameter space

Finally, concerning the symmetry aspects of the model Hamiltonian, we also mention that there occur special transformation that act only in the parameter space. Indeed, one can identify reflection-like relations in the parameter space of the Hund and spin-orbit couplings (J_H,λ) which can be expressed by the effective SU(2) operators $\mathcal{X}$ and $\mathcal{Y}$. The explicit form of the parameters space reflection symmetries is reported in the Appendix C.

D. Glide symmetry and multiple band touching points

A very distinct feature of the glide symmetry is that it can lead to multiple band touching points. Due to the intrinsic dependence on $k_2/2$ in $\mathcal{R}^{t}_{k_1,k_2}$ the diagonal blocks $H^{\pm}_{0(\pi),k_2}$ of the Hamiltonian in the glide line, for each glide eigenvalue $g = \pm 1$, have the following properties: (i) they are 4π periodic and (ii) related by a 2π shift because the whole spectrum must be 2π periodic, i.e., $H^{+}_{0(\pi),k_2} = H^{-}_{0(\pi),k_2+2\pi}$. Despite the fact that the eigenvalues of $H^{\pm}_{0(\pi),k_2}$ are 4π periodic it may occur that the determinant of the glide block has a shorter period of 2π for a given value of μ, i.e., $\det(\mathrm{H}^{+}_{0(\pi),k_2} - \mu) \equiv \det(\mathrm{H}^{+}_{0(\pi),k_2+2\pi} - \mu)$. The consequence of such invariance is that if at $k_2 = k_0$ one or more than one band crosses the Fermi level μ then it implies that the Fermi level will be crossed as well at $k_2 = k_0 + 2\pi$. We observe that such property is not related to the degeneracy of the second Fermi point or to the origin of a given band crossing the Fermi level at k_0. Now, if we combine the two glide blocks, we have that the 2π-shift invariance of the determinant plus the 2π-shift relation between $g = +1$ and $g = -1$ glide blocks make the Fermi points from opposite g sectors to fall on top of each other. Then, the whole spectrum will exhibit a multiple band touching both at k_0 and $k_0 + 2\pi$. This mechanism is schematically depicted in Fig. 4. In the following sections, we will show that such a situation is not rare and, indeed, it happens in a broad parameter range for the $z3$ configuration, both for zero or a finite value of μ. In Appendix D, we show that such mechanism can also apply to other zigzag configurations.

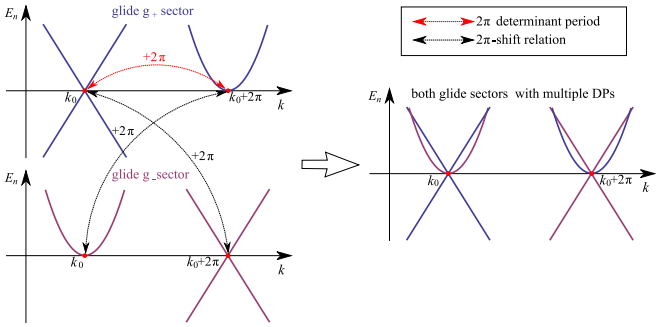

FIG. 4. Schematic description of the mechanism for the generation of multiple degenerate band crossings as due to the 2π periodicity of the determinant in each glide block $g = \pm 1$ and 2π shift relation between the glide block Hamiltonians.

IV. RESULTS

In this section, we present the electronic phase diagram associated to the $z2$ and $z3$ configurations, being those more relevant for the materials perspective. We select representative electron filling cases to highlight the most interesting electronic structures which can be achieved. The aim is to firstly consider which type of electronic states can be obtained and how they vary as a consequence of the interplay between the spin-orbit and Hund coupling. Then, taking as a guide the discussion on the symmetry properties of the system, we determine and discuss the most relevant features of the electronic spectra and the related edge states for given slab geometries. The analysis hence points to investigate the possibility of having topological nontrivial configurations with a special focus on the interplay among the various symmetries that can play a role in protecting the gapless states.

A. Phase diagram and topological features of the insulating states

We start by considering the electronic phase diagram due to the competition of the Hund and spin-orbit couplings as a guide of the possible configurations that can be obtained in the model system. A distinct feature that we get from the determination of the phase diagram in Fig. 5 is that both spin-orbit coupling and Hund interaction are able to drive a (semi)metal-to-insulator transition. Indeed, large λ or J_H can lead to insulating configurations that can be generally ascribed to the formation of almost disconnected orbital molecules made of locally spin-orbit mixed $d_{xz/yz}$ bands or developing within the zigzag segments due to the orbital directionality of the itinerant bands [33]. Hence the relative ratio of the SOC and Hund coupling can drive a series of (semi)metal-insulator transitions where different types of gapless phases occur in between the insulating states as demonstrated for two representative electron densities in Figs. 5(a) and 5(b). We observe that the gapless phases can be rather robust to variation of the microscopic parameters. Another interesting aspect that we extract from the investigation of the electronic phase diagram is that the semimetal states can have Dirac points along the mirror lines, in the glide symmetric lines, or in a generic position of the BZ (this happens for instance for the half-filling $z2$ phase, not shown here), thus indicating

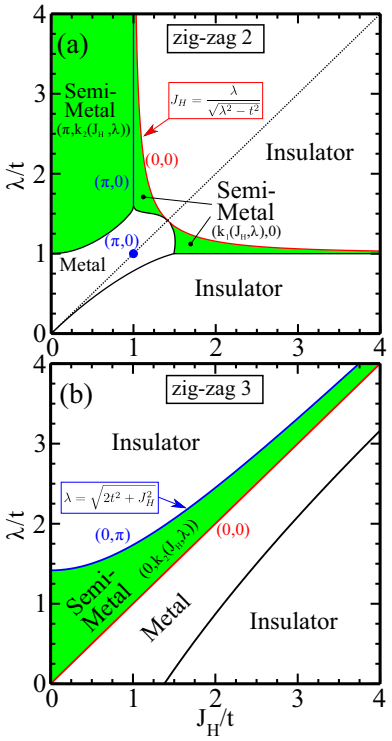

FIG. 5. Phase diagrams for (a) $z2$ magnetic state at 3/4 filling and (b) $z3$ configuration at half filling. Topological semimetal phases are marked with color (green area) and the position of Dirac points in the BZ is reported in parenthesis. Red and blue lines indicate configurations where the DPs are in high symmetry positions. Analytical dependence of nontrivial phase boundaries is also explicitly shown.

that both nonspatial and spatial symmetries play an important role in determining the character of the electronic structure. Indeed, in the case of $z2$, by varying the Hund coupling at a given λ, one can first get a transition from a semimetal phase with Dirac points lying in the glide symmetric line at $k_1 = \pi$ to Dirac points in the mirror line at $k_2 = 0$, and then, above a critical J_H, the merging of the Dirac points at a high symmetry position leads to a gap opening in the insulating phase. We observe that for $z2$ it turns out to be difficult to access the insulating phase from semimetal state with Dirac points in the glide plane [Fig. 5(a)]. This is different from the case of $z3$ where a direct glide semimetal to insulating state can be obtained by varying either the spin-orbit or the Hund coupling. These aspects anticipate a qualitative difference between the electronic states in the two considered cases that we will analyze in more details below.

Moreover, we observe that along the diagonal of the phase diagram a semimetal phase can be achieved with DPs always lying in one of the glide plane, i.e., at $k_1 = 0$. Such finding is specific of the model Hamiltonian and is a consequence of a symmetry in the parameter space that interchanges J_H with λ or J_H with $-\lambda$ in $\mathcal{H}_{\vec{k}}$, as also described in more details in Appendix C.

Concerning the topological properties of the resulting electronic phases, we firstly deal with some general considerations on the fully gapped insulating phases. Taking into account

the symmetry analysis in the Sec. III, we observe that time reversal $\mathcal{T}$ with $\mathcal{T}^2 = 1$ is the internal symmetry of the model Hamiltonian. Then, for time conserving configurations, the system is in the AI class of the tenfold Altland-Zirnbauer (AZ) classification table [82]. According to the AZ topological classification, in two-dimensions the fully gapped states cannot have any topological protection due to the nonspatial symmetries and, indeed, we do not find any edge state occurring when considering a ribbon geometry with open boundary along any given direction. On the other hand, for broken time reversal symmetry one can have insulators with nontrivial Chern numbers as well as gapless phases (Fermi lines or points) with nontrivial topological invariants, being allowed in the A class [83].

The presence of symmetries that act nonlocally in position space can in principle expand the possibilities of having nontrivial topological configurations both for the insulating and the gapless phases. The analysis of the electronic structure indicates that there are no evidence for non trivial edge states. Such result is consistent with the expectations for the AI class that the insulating phase in two-dimension are always trivial both in the presence of mirror symmetry [83] or nonsymmorphic transformations compatible with the model system, as indicated in the Sec. III on the symmetry properties [62]. Hence, on the basis of this result and taking into account the phase diagram for the $z2$ and $z3$ states, the following analysis is mainly concentrated on the character of the gapless states.

B. Gapless phases of zigzag $z2$ antiferromagnet

We start by considering the $z2$ AFM and the semimetal phases with DPs in the glide plane. There are various distinct aspects related to the analysis of such electronic configuration. On one hand, the semimetal phase exhibits a rather strong stability in the phase diagram. On the other hand, it represents a good candidate to get a deeper insight on the role of the nonsymmorphic glide transformation and its interplay with the other symmetries which are present in the model system. Indeed, interestingly, we find that not only the glide, but also the inversion, and combination of inversion with time-reversal emerge as relevant symmetries for protecting the semimetal phase.

To set the stage we select a point in the phase diagram of Fig. 5(a), which is representative of the electronic states at large spin-orbit coupling. For such case, the energy spectra in the whole BZ are shown in Fig. 3(a) and we can see that two Dirac points occur in the glide line at $k_1 = \pi$. Since the glide operator $\mathcal{R}^t_{k_2}$ commutes with $\mathcal{H}_{\vec{k}}$ in the glide line, the electronic states can be labeled by the $g = \pm 1$ glide eigenvalues. The DPs occur at the crossing of the bands with opposite g and they are then protected by the glide symmetry [as shown in Fig. 6(a)]. Hence, we determine the edge states by considering a ribbon geometry with open edge parallel to the vector $\hat{a}_1$. As demonstrated in the Fig. 6(c), we have two degenerate and dispersive states that are strongly localized on the left and right boundary of the ribbon, respectively. Since for such configuration the momentum k_1 is conserved, in the figure the two DPs fall on top of each other at $k_1 = \pi$.

To better understand the nature of the resulting edge states, one can employ an alternative configuration with open edge parallel to $\hat{a}_2$. In Fig. 6(d), we provide the spectrum of such ribbon geometry indicating that the two edge states now connect the two DPs located at $k_2 = k_0$ and $k_2 = 2\pi - k_0$ and they are not degenerate any more. We find that in general the $\hat{a}_2$ direction is more dispersive than the $\hat{a}_1$. This is expected because the electronic propagation, due to Hund's coupling, is more favorable along the zigzag path rather than across them. Another explicit outcome is that all the states depicted in Fig. 6(d) have a finite probability of being localized on the edge of the ribbon whereas almost all the states in Fig. 6(c) tend to avoid the edges, as one can infer from the spectral weight distribution (see the color map in the figure). A closer inspection of Fig. 6(d) also indicates that apart from having two edges states between the two DPs there is one extra edge mode connecting them through the zone boundary. To understand the presence of this mode it is important to consider a different mechanism of symmetry protection of the DPs besides the glide symmetry.

Indeed, from the structure of the glide operator $\mathcal{R}^t_{k_2}$ we deduce that, for a fixed k_2, it has the standard form (i.e., k-independent) of an inversion operator for a family of effective one-dimensional (1D) subsystems that are gapped as long as $k_2 \neq k_0, 2\pi - k_0$. Taking into account the discussion of Sec. III C, we know that the projected Hamiltonians within the k_2 cuts are time-reversal invariant and belonging to the AI class. Thus, for each gapped cut, one can define an inversion topological number $\mathbb{Z}^{\geqslant}$ [85] which is due to the difference of the number of occupied states with a given inversion eigenvalue at the two inversion invariant points, i.e., at $k_1 = 0$ and $k_1 = \pi$. Hence, from the spectra in the $g = +1$ glide sector at $k_1 = \{0, \pi\}$ shown in Fig. 6(b), one can see that $\mathbb{Z}^{\geqslant}$ changes sign at the position of the DPs, i.e., both at k_0 and $2\pi - k_0$. Such findings imply that at these points we have a topological phase transition between trivial and nontrivial 1D cuts which require a gap closing, that is indeed obtained at the DPs. The mechanism described above explains the presence of a third edge state close to the zone boundary in Fig. 6(d) because for such values of k_2 we are in the the nontrivial cuts for the projected Hamiltonian.

Now, we demonstrate that the gap closing due to the inversion driven topological transition in the 1D cuts with fixed k_2 can also occur in the absence of glide symmetry. For this purpose, in Fig. 6(e), it is reported the spectrum of a system with open edge along $\hat{a}_1$ with broken glide and mirror symmetry but preserved inversion. In order to achieve an electronic state with such symmetry conditions, we introduce anisotropy by unbalancing the hopping in the $\hat{a}$ direction with respect to that in $\hat{b}$. The outcome is that the DPs do not get gapped but they move away from the glide plane. In the absence of glide symmetry, $\mathbb{Z}^{\geqslant}$ can be defined only in the two high-symmetry cuts of the BZ, i.e., at $k_2 = \{0, \pi\}$, where the global inversion $\mathcal{I}_{\vec{k}}$ is equivalent to the 1D inversion symmetry within the cut. Thus, according to Fig. 6(b) for $k_2 = 0$, we have a topologically nontrivial state which becomes trivial at $k_2 = \pi$. Due to the inequivalent topological character, there must be a gap closing between these two 1D lines and this is indeed the reason for which the DPs in Fig. 6(e) are still preserved.

Finally, the investigated $z2$ state can also exhibit a symmetry protection arising from the combination of $\mathcal{I}$ and $\mathcal{T}$. Their product yields a conjugation operator $\mathcal{K}$ as described in Sec. III C. Due to the presence of the $\mathcal{K}$ symmetry, $\mathcal{H}$

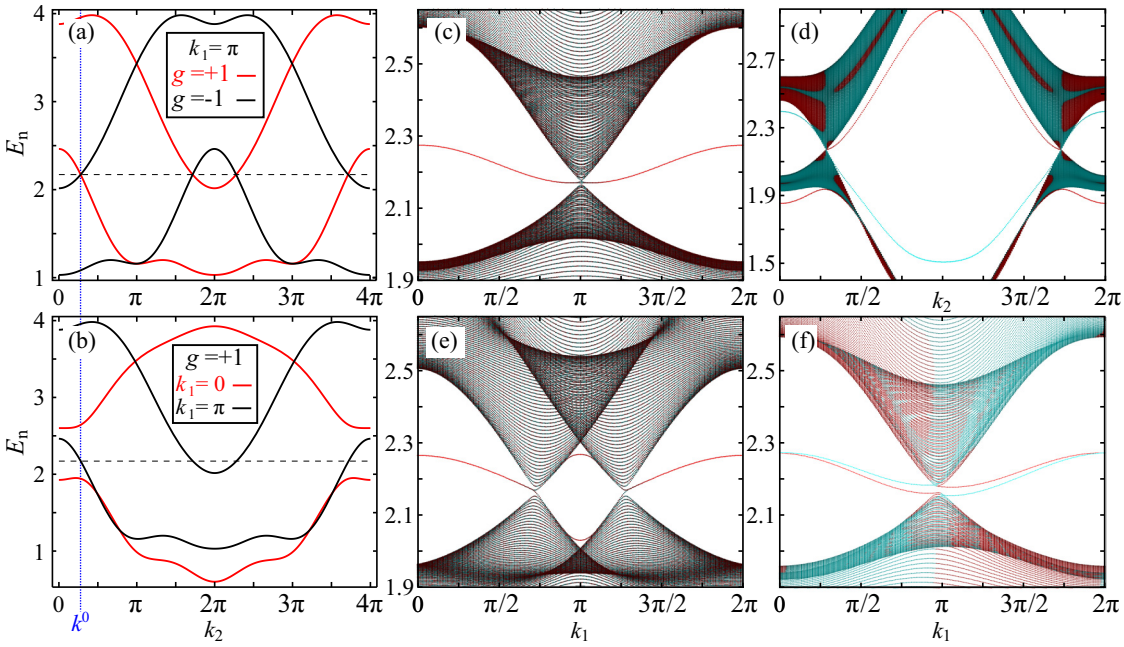

FIG. 6. Electronic spectra for $z2$ AF at 3/4 filling. (a) Band structure in the glide plane at $k_1 = \pi$, with glide eigenvalues $g = +1$ (red) and $g = -1$ (black), and (b) $g = +1$ glide symmetric bands at $k_1 = 0$ (red) and $k_1 = \pi$ (black) as functions of k_2. Dashed line sets the Fermi level. (c)–(f) one-dimensional spectra and edge states for a slab geometry with open boundary. Spectra for a slab configuration with open boundary in the (c) $\hat{a}_1$ and (d) $\hat{a}_2$ directions, with k_1 and k_2 being the momentum parallel to the edge, respectively. Electronic spectra with (e) open boundary along $\hat{a}_1$, broken glide and reflection symmetries with inversion invariance, and (f) with only broken time-reversal. Color map of the 1D spectra with high (low) brightness indicates a large (small) probability of the electronic states to be localized on the left (red) or right (blue) boundary.

can be made purely real in the eigenbasis of $\mathcal{K}_{\vec{k}}$. Indeed, close to the DPs, the low-energy Hamiltonian has a form $H_{\delta\vec{k}} = \delta k_1 A + \delta k_2 B$ with A and B being 2×2 real matrices and $\delta\vec{k}$ the deviation with respect to the DP. We can then calculate a $\mathbb{Z}_2^{(1)}$ mod-2 winding number around each DP and it takes values ± 1 at the two DPs.

In order to explicitly compute the invariant, one can use an approach based on the Green's function [84]. Indeed, we define the Green's operator $\mathcal{G}$ as

$$\mathcal{G}(\omega,k) = \frac{1}{i\omega - \mathcal{H}_{\vec{k}}}, \tag{49}$$

where the Fermi energy is at $\omega = 0$. The $\mathbb{Z}_2$ topological numbers of the first generation $\mathbb{Z}_2^{(1)}$ are defined in a similar way as those associated to the $\mathbb{Z}$ numbers but they usually require an extension of the Hamiltonian (or the Green's function). This extension involves an auxiliary parameter $u \in [0,1]$ which becomes an extra dimension to be integrated over. The extended Hamiltonian has a form $\tilde{\mathcal{H}}_{\vec{k}} = (1-u)\mathcal{H}_{\vec{k}} + u\mathcal{H}_0$, where $\mathcal{H}_0$ is a trivial Hamiltonian with energies $\pm E_0$. From the extended Hamiltonian $\tilde{\mathcal{H}}$, we deduce the Green's function $\tilde{\mathcal{G}}$. The $\mathbb{Z}_2^{(1)}$ topological number $N_p^{(1)}$ of the Fermi surface with codimension p is then given by

$$N_p^{(1)} = C_p' \int_{S^p} \int_0^1 \mathrm{d}u\ \mathbf{tr}[(\tilde{\mathcal{G}}\mathrm{d}\tilde{\mathcal{G}}^{-1})^p \tilde{\mathcal{G}}\partial_u\tilde{\mathcal{G}}^{-1}] \bmod 2, \tag{50}$$

with a prefactor

$$C_p' = -\frac{2(p/2)!}{p!(2\pi i)^{p/2+1}} \tag{51}$$

and p being the difference of the system's dimension d and the dimension d_{FS} of the Fermi surface. Thus the $\mathbb{Z}_2^{(1)}$ number is nonvanishing only for even codimension p. In our case, this formula is applied to calculate the topological charges of the Dirac points in two dimensions- $p = 2$. It is worth to mention that in this case, since we deal with a purely real 2×2 Hamiltonian, the extension $\mathcal{H}_0$ must be chosen as imaginary to get a nonvanishing $N_p^{(1)}$, here, $\mathcal{H}_0 = \sigma^y$ is selected. The computation of $\mathbb{Z}_2^{(1)}$ yields values ± 1 at the two DPs. Though the combined time-inversion operator $\mathcal{K}$ is explicitly dependent on the momentum, due to its nonsymmorphic nature, in the low-energy description the result is consistent with the general expectation [89] of having a nontrivial $\mathbb{Z}_2$ topological invariant at the DPs by combination of time and inversion symmetry.

Hence we conclude that the analysis of the electronic spectra for the $z2$ phase in Fig. 6 indicates a peculiar character of the semimetal phase and accordingly of the edge modes as due to the interplay of the glide with other combined symmetries, being robust to different types of symmetry breaking configurations.

Concerning the general expectation out of the application of lowering symmetry perturbations, due to the presence of different protections there are various paths to reach a less symmetric state for which the topological protection can be preserved or destroyed. For instance, breaking of the glide symmetry in such a way that inversion is not preserved will split the DPs, opening a gap, and the system becomes topologically trivial. Such result is consistent with the prediction from the AZ classification table for the AI class

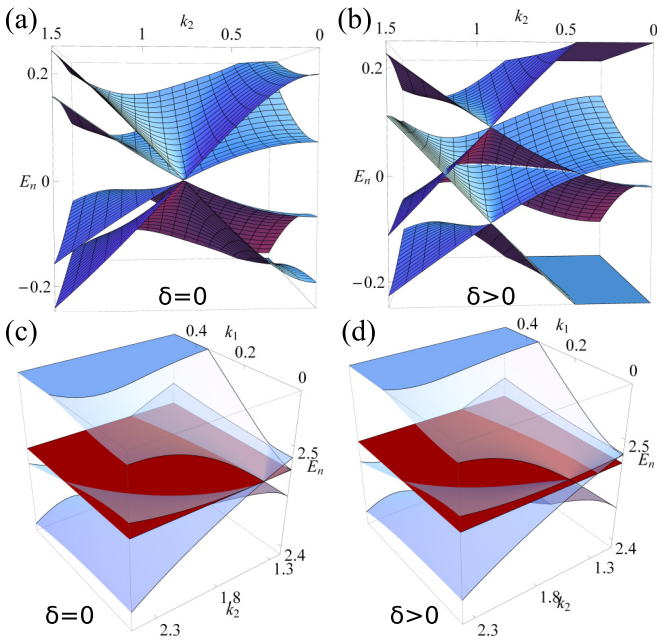

FIG. 7. Electronic spectra around the Fermi level and $k_1 = 0$ in the glide line for $z3$ configurations at (a) and (b) half-filling and (c) and (d) $\mu = \mu_0$. Bands are plotted as semitransparent in panel (c) and (d), while the Fermi level is indicated by the red plane. At half-filling, the system evolves from point node semimetal (a) at $\delta = 0$ to a line-node semimetal made of semi-Dirac points (b) at $\delta > 0$. At $\mu = \mu_0$, the evolution is from a metallic configuration having a triple degenerate Fermi point (c) at $\delta = 0$, to a multi Fermi pockets metallic state (d) at $\delta > 0$.

in the presence of a mirror reflection [83]. Otherwise, breaking of the reflection or time only removes the $\mathbb{Z}_2$ protection but leaves the glide symmetry so that the semimetal phase and the DPs are still preserved. In Fig. 6(f), a representative case of time-reversal violation is also considered. Here, we only highlight the possibility of having, in the presence of time reversal symmetry breaking, nondegenerate chiral states at the edge. Due to a termination dependent orbital polarization, the edge modes can sustain both charge and orbital polarized currents at the boundary.

C. Gapless phases of zigzag $z3$ antiferromagnet

Let us consider the $z3$ antiferromagnetic case. As for the other zigzag magnetic patterns, the main aim is to focus on the character of the gapless phases with respect to the glide symmetry and its interplay with the other symmetries of the model system. Though, there is a large variety of electronic states that can be achieved by varying the spin-orbit, the Hund coupling or the hopping connectivity, the $z3$ pattern allows to observe peculiar types of gapless phases, which uniquely emerge in conjunction with the presence of the glide symmetry.

In Figs. 7(a) and 7(c), we observe that the gapless phases in the glide plane exhibit quadruple and triple band touching at half-filling and away from it at a given value of $\mu = \mu_0 = \sqrt{2 + J_H^2 + \lambda^2}$.

At half-filling, we have a semimetal state with two DPs that are merged while at $\mu = \mu_0$, the triple point is attached to a Fermi pocket. Such feature of the electronic spectra is more explicitly evident if one projects the spectra in the glide plane at $k_1 = 0$. We can observe that quadruple band crossings are obtained at different values of k_2 at half-filling [Fig. 8(a)] while triple band crossings occur for the electron filling corresponding to μ_0 [Fig. 8(d)]. The construction of glide symmetric eigenstates [i.e., red and black lines in Fig. 8(a) and 8(d)] in the glide line allows to see that there are independent crossings in each glide block and that, due to the glide symmetry, a shift of 2π connects inequivalent eigenstates within each glide sector. In order to better clarify the nature of such multiple band touchings, it is convenient to introduce a symmetry conserving term in the Hamiltonian by modifying the hopping connectivity through the next-nearest neighbor hopping δ. The application of δ leads to a splitting of the quadruple and triple band touchings [Figs. 7(b), 7(d), 8(b), and 8(e)] thus revealing that the multiple degeneracy is not associated to the symmetry properties discussed in the Sec. III but rather to another emerging property of the Hamiltonian. Indeed, a closer inspection of the electronic structure in the two glide sectors indicates the origin of the multiple band crossings. The key issue here is that there is a nonunitary transformation that leaves invariant the determinant of the glide-block Hamiltonian H^+_{0,k_2} with respect to a 2π shift in the momentum. Then, taking into account the general arguments of Sec. III D we can have that the Fermi points exhibit a multiple degeneracy. It is important noticing that such property of the determinant is not tied to the chiral symmetry of the spectrum, because it manifests itself both at $\mu = 0$ and μ_0, respectively. The anomalous periodicity of the determinant can be constructed explicitly, as demonstrated in Appendix D, through a nonunitary chiral-like operator $\Sigma_{k_2} \equiv h^{-1}_{k_2} \bar{H}_{k_2}$ where $\bar{H}_{k_2}$ is the 2π periodic part of H^+_{0,k_2} and h_{k_2} is the part with 4π period ($h_{k_2+2\pi} \equiv -h_{k_2}$). The proof relies on the fact that eigenvalues of Σ_{k_2} are symmetric around zero and on the Silvester property of determinants, i.e., $\det(1 + \mathrm{AB}) \equiv \det(1 + \mathrm{BA})$.

When breaking the conditions for the determinant invariance in the glide sectors, the DPs can split into simple DPs. This indeed happens when we introduce the hopping δ which does not break any symmetries of the system. The removal of degeneracy drives different type of transitions. At half-filling, it is concomitant with a changeover from a point node semimetal to a gapless phase built by a line of semi-Dirac points as shown in Fig. 7(b). Otherwise, the metal coexisting with a triplet band crossing Fermi point is converted into a metallic configuration whose electronic structure is tied to the presence of topological nontrivial DPs in the glide plane.

Concerning the issue of the symmetry protection and the topological character, let us start from the chiral case at half-filling where δ can induce a transition from a point node to a line node semimetal (Fig. 7). At $\mu = 0$ and finite δ, the line of semi-DPs has a topological nature which is related to the glide symmetry and the nonsymmorphic nature of the chiral symmetry. Indeed, as shown in the Sec. III, by combining the chiral and the conjugation symmetries we find a k-dependent anticonjugation operator $\mathcal{A}_{\vec{k}}$, which acts to give a minus complex conjugate of $\mathcal{H}_{\vec{k}}$. We point out that due to its nonsymmorphic character, such symmetry is not explicitly included in the topological classification of the

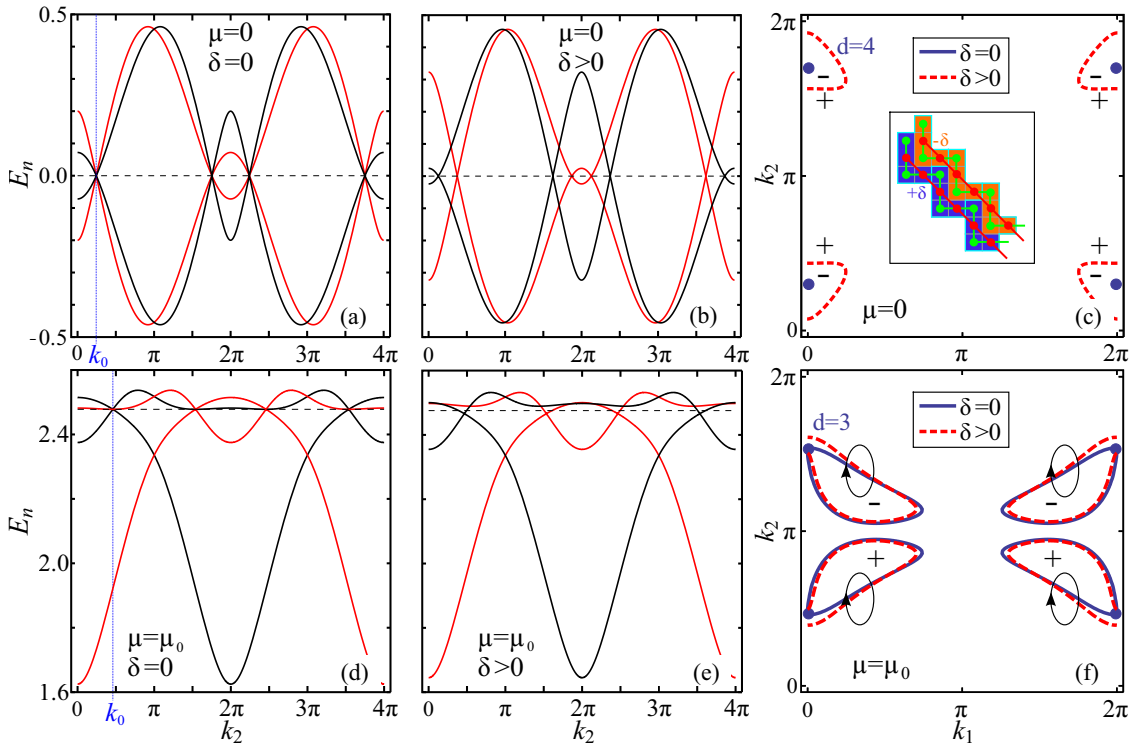

FIG. 8. Multiple FPs in $z3$ antiferromagnet. Bands in the glide plane $k_1 = 0$ at $\delta = 0$; (a) with chiral fourfold DPs at half-filling ($\mu = 0$) and (d) with threefold Fermi points at $\mu = \mu_0$. Color indicates the glide eigenvalue $g = +1$ (red) and $g = -1$ (black), dashed line is the Fermi level μ. (b) and (e) The same bands in presence of the symmetry conserving long-range hopping δ. (c) and (f) Fermi point node at $\delta = 0$ (blue) and line nodes at $\delta > 0$ (red dashed). Multiple band crossing points are marked with dots and their degeneracy is indicated in the corresponding color. The inset of (c) shows a schematic view of the hopping δ. The signs in (f) indicate the band parity, $+1$ inside the Fermi pockets and -1 outside. The signs in (h) are those due the AI winding numbers of the Fermi lines. The integration contours are indicated by ellipses.

one-dimensional Fermi lines by combination of particle-hole and inversion [89]. Taking into account the fact that $\mathcal{A}$ is real for odd L_z, as shown in Sec. III, we can put the Hamiltonian in a purely imaginary and thus antisymmetric form using the eigenbasis of $\mathcal{A}_{\vec{k}}$. For an antisymmetric operator, we can construct a $\mathbb{Z}_2$-type topological invariant as a sign of its Pfaffian. The main result is that we can identify the nodal line by the position of the sign change of the Pfaffian of $\mathcal{H}_{\vec{k}}$ [Fig. 8(c)] thus indicating that the line of DPs exhibits a topological protection. Apart from the whole line of semi-DPs, one can notice that in the glide plane $k_1 = 0$ the $\mathcal{A}$ operator is not k-dependent because the chirality depends only on k_1, and, thus, it also provides a protection for the DPs in both glide sectors as an ordinary symmorphic product of inversion an particle-hole symmetry [89]. Then, if the nodal gapless state can be converted into a point node semimetal by suitably tuning the microscopic parameters, the transition can only occur in the glide plane and the semimetal phase will exhibit multiple degenerate DPs, as it happens for instance at $\delta = 0$. Such outcome can be generally expected for glide and chiral symmetric semimetal phases in AI class which exhibit a topological protection in the full BZ and in one of the glide lines. Interestingly, breaking of the glide symmetry opens a gap at the Fermi level everywhere in the BZ except the glide plane where the DPs can be still protected by the particle-hole and inversion combination as it is observed for the investigated electronic phases at half-filling. Therefore the overall character of the emerging gapless phase is to exhibit a topological protection and to be marked by two pockets of semi-DPs that are glued to the line at $k_1 = 0$ due to the glide symmetry protection.

When moving away from half-filling, e.g., at $\mu = \mu_0$, each Fermi pocket of the metallic phase can exhibit a protection due to a non trivial AI winding number $\mathbb{Z}$. Indeed, for the nonchiral case of a Fermi surface with a codimension p the topological number N_p can be expressed as an integral over an oriented manifold of the dimension p, e.g., a p sphere, in a $(\omega,\vec{k})$-space enclosing the Fermi surface,

$$N_p = C_p \int_{S^p} \mathbf{tr}[(\mathcal{G}\mathrm{d}\mathcal{G}^{-1})^p], \tag{52}$$

where the prefactor C_p is given by

$$C_p = -\frac{n!}{(2n+1)!(2\pi i)^{n+1}}, \tag{53}$$

with $p = 2n + 1$. Thus the formula is valid only for odd p and for even ones the $\mathbb{Z}$ topological number vanishes. Note that the power under the trace means an external product of p copies of $(\mathcal{G}\mathrm{d}\mathcal{G}^{-1})$. Since the problem is two-dimensional, we have $p = 1$ and thus we can get a nonvanishing N_p calculating the integral over a circle around the Fermi line. For simplicity, the circle can be chosen in the (ω,k_1) plane with a center belonging to the Fermi surface. Alternatively, one can notice that in such a low-dimensional case the expression (52) will

count the difference of number of occupied states on either side of a Fermi point. The computation of the topological number of the line Fermi surface associated to the pockets in Fig. 8(f) gives an alternating sign when moving along k_2. Hence, in general, we do not observe a semimetal phase and the triple band crossing coexists with the Fermi pockets [Fig. 7(d)] at $\delta > 0$.

V. CONCLUSIONS

We have investigated the nature and the symmetry properties of the electronic structure of a class of itinerant antiferromagnets where electrons with two-orbitals flavors are coupled to a magnetic background of localized spins that order in a zigzag pattern. The character of the antiferromagnetic pattern is a crucial ingredient that brings a series of nontrivial symmetry transformations which include also translation of fraction of a Bravais lattice vector. We provided a detailed description of the symmetry features of the model system and of the main consequences on the electronic states when considering the most relevant zigzag configurations. A particular aspect that arises from the analysis refers to the interplay of the nonsymmorphic glide symmetry and the other symmetries with spatial and internal character occurring in the model system.

While the possibility of having topological zigzag antiferromagnets and edge states has been mainly focusing on insulating configurations [87,88] and on the symmetry protection within one-dimensional projected electronic structures [86], our analysis demonstrates that the breakdown of the fully gapped phases in 2D multiorbital zigzag AFMs can yield a variety of nontrivial gapless phases. The character of these states depends on the characteristic zigzag length as well as on the intricate interplay of nonsymmorphic and internal or other spatial symmetries. Our results demonstrate that, for the considered class of two-dimensional zigzag AFMs with collinear magnetic order and time reversal invariance (i.e., in the AI symmetry class), gapless phases are prone to exhibit different sources of symmetry protection and a topological behavior. Indeed, we find that the fully gapped phases are in general topologically trivial and possible topological states can be achieved only by breaking the time reversal symmetry or in one-dimensional projections of the electronic spectra. On the other hand, when dealing for instance with $z2$ magnetic pattern, the Dirac points in the semimetal phases can exhibit robust symmetry protection as due to the glide symmetry and the combination of inversion with time or particle-hole.

Another distinct feature of our findings is provided by the invariance of the determinant in the glide sectors that points to an interesting mechanism, uniquely arising in nonsymmorphic systems, to generate multiple Dirac points. In this framework, we demonstrate that the breaking of an anitunitary nonsymmorphic chiral symmetry allows to have a unique transition from a semimetal to a line node gapless phase made of semi-Dirac points. This is a peculiar electronic feature that can manifest only for odd zigzag antiferromagnet as explicitly demonstrated according to the property of the symmetry transformation for the $z3$ configuration.

Finally, due to the symmetry protection of the Fermi points in the glide line and the strong nesting of the gapless phase, it is plausible to expect that the semimetal and metallic phases can exhibit anomalous magnetotransport response as well as a tendency to other electronic instabilities. Concerning the materials perspective, there are many compounds exhibiting zigzag magnetic patterns that involve t_{2g} orbitals close to the Fermi level especially when considering transition metal oxides. For instance, in this framework, our results may find interesting application both in Mn doped ruthenates and dichalcogenides.

ACKNOWLEDGMENTS

W.B. acknowledges support by the European Horizon 2020 research and innovation programme under the Marie-Sklodowska-Curie grant agreement No. 655515.

APPENDIX A: COMMUTATION RELATIONS OF SPATIAL AND NONSPATIAL SYMMETRIES

For the model system upon examination, it is not direct to predict if the reflection and the glide operators commute. In order to calculate their commutator, one has to carefully consider the relation with the Hamiltonian, so it is crucial to update the $\vec{k}$ points for which we consider the application of the symmetry operators. For instance, one can show that the operation of reflection and glide does not depend from their order with respect to the Hamiltonian which means that

$$\mathcal{R}_{k_2}\mathcal{R}^t_{k_1,-k_2} - \mathcal{R}^t_{k_1,k_2}\mathcal{R}_{k_2} \equiv 0. \tag{A1}$$

Thus, along this line, one can demonstrate that the inversion operator commutes with the above operators. Concerning the relation with respect to the time reversal operation one finds that both normal reflection and glide commute with $\mathcal{T}$, that is,

$$\mathcal{R}_{k_2}\mathcal{T} - \mathcal{T}\mathcal{R}^\star_{-k_2} \equiv 0 \tag{A2}$$

and

$$\mathcal{R}^t_{k_1,k_2}\mathcal{T} - \mathcal{T}\mathcal{R}^{t\star}_{-k_1,-k_2} \equiv 0, \tag{A3}$$

where the symbol star indicate complex conjugation. Thus we conclude that the same property holds for the inversion. Finally, concerning the chirality (sublattice) symmetry, we find that the reflection commutes with $\mathcal{S}_{k_1}$,

$$\mathcal{R}_{k_2}\mathcal{S}_{k_1} - \mathcal{S}_{k_1}\mathcal{R}_{k_2} \equiv 0, \tag{A4}$$

and the glide anticommutes or commutes with $\mathcal{S}_{k_1}$ for even or odd L_z respectively, i.e.,

$$\mathcal{R}^t_{k_1,k_2}\mathcal{S}_{k_1} + (-1)^{L_z}\mathcal{S}_{k_1}\mathcal{R}^t_{k_1,k_2} \equiv 0. \tag{A5}$$

One can also intuitively argue that the chiral symmetry is related to the two-sublattice structure of the model system. Since under a reflection transformation a site belonging to one sublattice goes into another site of the same sublattice we get a vanishing commutator in (A4). On the other hand, looking at Fig. 2, we notice that for $L_z = 2$ the glide does mix the sites from different sublattices hence one gets a vanishing anticommutator. It is easy to check that this happens for any even L_z whereas for the odd ones we always get a vanishing commutation relation. Finally, we note that since all spacial symmetries commute with time reversal, their commutation

relation with particle-hole symmetry is the same as that one with the chirality.

APPENDIX B: k-DEPENDENT GAUGE TRANSFORMATIONS

As we noticed in the previous sections, due to the structure of the unit cell and the presence of the nonsymmorphic glide symmetry, most of the spatial and nonspatial symmetries are k-dependent. It is worth and interesting to underline that these k dependencies can be gauged away simultaneously or separately by for any zigzag segment length L_z by proper k-dependent gauge transformations. In the following sections, we will show how to get rid of k dependence from; all symmetries in Sec. B 1 and reflection only in Sec. B 2. In Sec. B 3, we show how to reduce the k dependence in glide only to the k component related to the shift along the glide plane.

1. k-independent all symmetries

To make all symmetries simultaneously k-independent, we define a following gauge transformation $\mathcal{G}_{\tilde{k}}$:

$$\mathcal{G}_{\tilde{k}} = \begin{pmatrix} \mathbf{G}_\downarrow & \mathbf{0} & \mathbf{0} & \mathbf{0} \\ \mathbf{0} & \mathbf{G}_\uparrow & \mathbf{0} & \mathbf{0} \\ \mathbf{0} & \mathbf{0} & \mathbf{G}_\downarrow & \mathbf{0} \\ \mathbf{0} & \mathbf{0} & \mathbf{0} & \mathbf{G}_\uparrow \end{pmatrix}, \tag{B1}$$

with diagonal blocks $\mathbf{G}_\downarrow$and $\mathbf{G}_\uparrow$ of the size $N_\downarrow = N_\uparrow = 2L_z - 2$,

$$\mathbf{G}_\downarrow = e^{-ik_1} \begin{pmatrix} 1 & 0 & 0 & \cdots & 0 \\ 0 & e^{i\frac{1}{N_\downarrow}k_2} & 0 & \cdots & 0 \\ 0 & 0 & e^{i\frac{2}{N_\downarrow}k_2} & \cdots & 0 \\ \vdots & \vdots & \vdots & \ddots & 0 \\ 0 & 0 & 0 & 0 & e^{i\frac{N_\downarrow-1}{N_\downarrow}k_2} \end{pmatrix}, \tag{B2}$$

and

$$\mathbf{G}_\uparrow = e^{i\frac{k_1}{2}}\mathbf{G}_\downarrow, \tag{B3}$$

corresponding to the domains of spin up/down in the unit call. Note that these matrices are the same for the orbital a and orbital b sector. The Hamiltonian transforms as a linear operator under the basis rotation, i.e.,

$$\tilde{\mathcal{H}}_{\tilde{k}} \equiv \mathcal{G}^\dagger_{\tilde{k}}\mathcal{H}_{\tilde{k}}\mathcal{G}_{\tilde{k}}, \tag{B4}$$

where tilde indicates the operator in the gauge transformed basis. Now, if we require that the reflection operator in the gauge transformed basis, i.e., $\tilde{\mathcal{R}}$ acts as a reflection operator with respect to $\tilde{\mathcal{H}}_{\tilde{k}}$, i.e.,

$$\tilde{\mathcal{R}}^\dagger\tilde{\mathcal{H}}_{k_1,k_2}\tilde{\mathcal{R}} = \tilde{\mathcal{H}}_{k_1,-k_2}, \tag{B5}$$

we easily find that $\tilde{\mathcal{R}}$ should have the following form:

$$\tilde{\mathcal{R}} \propto \mathcal{G}^\dagger_{k_1,k_2}\mathcal{R}_{k_2}\mathcal{G}_{k_1,-k_2}, \tag{B6}$$

where the complex prefactor can be chosen in such a way to completely remove any k-dependence in $\tilde{\mathcal{R}}$. Similarly, we can proceed for the glide,

$$\tilde{\mathcal{R}}^t \propto \mathcal{G}^\dagger_{k_1,k_2}\mathcal{R}^t_{k_1,k_2}\mathcal{G}_{-k_1,k_2}, \tag{B7}$$

and for the other nonspatial symmetries. For instance, time reversal operator,

$$\tilde{\mathcal{T}} \propto \mathcal{G}^\dagger_{k_1,k_2}\mathcal{T}\mathcal{G}^\star_{-k_1,-k_2}, \tag{B8}$$

where the gauge matrix on the right is taken with complex conjugate. While for the chirality we have that

$$\tilde{\mathcal{S}} \propto \mathcal{G}^\dagger_{k_1,k_2}\mathcal{S}_{k_2}\mathcal{G}_{k_1,k_2}, \tag{B9}$$

and transforms through a simple basis rotation. The rest of the symmetries can be constructed by taking the product of the above operators, i.e.,

$$\tilde{\mathcal{I}} = \tilde{\mathcal{R}}\tilde{\mathcal{R}}^t = \tilde{\mathcal{R}}^t\tilde{\mathcal{R}}, \tag{B10}$$

to get the inversion and

$$\tilde{\mathcal{C}} = \tilde{\mathcal{T}}\tilde{\mathcal{S}}^\star = \tilde{\mathcal{S}}\tilde{\mathcal{T}}, \tag{B11}$$

to get charge conjugation. Note that the spatial symmetries and the time reversal do not transform as linear operators under basis rotation. For this reason their spectra are different in the gauge transformed basis with respect to the initial one and their commutation relations could be different as well. Accidentally, we find that the commutation relations remain the same as shown in previous section.

Finally, we stress that the consequence of the removal of the k dependencies from the symmetries operators is to alter the periodicity of the Hamiltonian in the momentum space. One finds that for a given L_z the period in k_1 is always doubled, i.e., $\tilde{\mathcal{H}}_{k_1+4\pi,k_2} = \tilde{\mathcal{H}}_{k_1,k_2}$ whereas that one in k_2 is increased $N_\downarrow$ times. This effect can be captured by what we call the *shift* operator. We find that however the period is elongated the old period of 2π survives up to a basis rotation described by a unitary shift operator χ. For k_1, we find that

$$\tilde{\mathcal{H}}_{k_1+2\pi,k_2} = \chi_1^\dagger\tilde{\mathcal{H}}_{k_1,k_2}\chi_1, \tag{B12}$$

where χ_1 can be found as a 2π-basis mismatch of the gauge matrix, i.e.,

$$\chi_1 \propto \mathcal{G}^\dagger_{k_1,k_2}\mathcal{G}_{k_1+2\pi,k_2}. \tag{B13}$$

One finds that

$$(\chi_1)^2 = 1, \tag{B14}$$

meaning that after two 2π shifts in k_1 we recover the same Hamiltonian $\tilde{\mathcal{H}}_{k_1,k_2}$. Similarly, for k_2, we observe

$$\tilde{\mathcal{H}}_{k_1,k_2+2\pi} = \chi_2^\dagger\tilde{\mathcal{H}}_{k_1,k_2}\chi_2 \tag{B15}$$

with χ_2 is the unitary shift operator having the form of

$$\chi_2 \propto \mathcal{G}^\dagger_{k_1,k_2}\mathcal{G}_{k_1,k_2+2\pi} \tag{B16}$$

and becoming unity after $N_\downarrow$ applications:

$$(\chi_2)^{N_\downarrow} = 1. \tag{B17}$$

2. k-independent reflection

The gauge transformation described in Sec. B 1 makes all the symmetry operators k-independent but concomitantly one has to increase the effective BZ of the Hamiltonian. This is caused by the fact that the unit cell is not left invariant by any of the symmetries of the whole system. In the case of glide, inversion, and chirality symmetries it is in indeed impossible to define a unit cell that would map onto itself under their action. However, in the case of reflection, this transformation is possible. Another operating scheme would be to choose a square unit cell, which is a 4×4 cell both for $z2$ and $z3$, but in this way we increase the dimensionality of the operators and create artificial symmetries coming from the multiple copies of the elementary cell. The other solution, which is much more convenient, is to slightly modify the elementary unit cell shown in Fig. 2. One has to remind that every physical site in the lattice has two orbital flavors so the resulting system can be also mapped into an effective bilayer. The reflection can be seen as a π-rotation of the bilayer with axis along the $\vec{a}_1$ direction. Thus a reflection-invariant unit cell can be constructed by taking the original cell for orbital b and for orbital a one has to move the first two sites ($i = 1,7$ in Fig. 2) of the vertical segments after the last two sites ($i = 6,12$ in Fig. 2) of the horizontal segments. This can be realized by a gauge transformation of the type

$$\mathcal{G}^{\mathcal{R}}_{k_2} = \begin{pmatrix} \mathbf{1}^b_{\downarrow} & \mathbf{0} & \mathbf{0} & \mathbf{0} \\ \mathbf{0} & \mathbf{1}^b_{\uparrow} & \mathbf{0} & \mathbf{0} \\ \mathbf{0} & \mathbf{0} & \mathbf{G}^R_{\downarrow} & \mathbf{0} \\ \mathbf{0} & \mathbf{0} & \mathbf{0} & \mathbf{G}^R_{\uparrow} \end{pmatrix}, \tag{B18}$$

with two identical subblocks for orbital a segment,

$$\mathbf{G}^R_{\downarrow,\uparrow} = \begin{pmatrix} e^{-ik_2} & 0 & 0 & \cdots & 0 \\ 0 & 1 & 0 & \cdots & 0 \\ 0 & 0 & 1 & \cdots & 0 \\ \vdots & \vdots & \vdots & \ddots & 0 \\ 0 & 0 & 0 & 0 & 1 \end{pmatrix}, \tag{B19}$$

carrying the gauge for the first sites of the vertical segment. After the covariant transformation of the reflection operator, i.e., $\mathcal{R}_{k_2} \to \mathcal{G}^{\mathcal{R}\dagger}_{k_2} \mathcal{R}_{k_2} \mathcal{G}^{\mathcal{R}}_{-k_2}$ and extracting global phase factor we find it completely k-independent.

3. k_1-independent glide

Another gauge transformation can be found to demonstrate that the glide operator $\mathcal{R}^t_{\vec{k}}$ is dependent only on k_2 without affecting the periodicity of the Hamiltonian. Again, this solution is equivalent to a modification of the elementary unit cell shown in Fig. 2. Treating the a and b orbital degrees of freedom as two layers one can treat the glide as a π rotation of the bilayer with axis along the $\vec{a}_2$ direction followed by a shift of $\vec{a}_2/2$. Thus a way to construct a unit cell, which is mostly compatible with a glide is to take the original cell for the orbital a and for the orbital b, and then shift the spin down domain by $\vec{a}_1$ (see Fig. 2). In this way we obtain a gauge transformation of the form

$$\mathcal{G}^{\mathcal{R}^t}_{k_1} = \begin{pmatrix} \mathbf{G}^{R^t}_{\downarrow} & \mathbf{0} & \mathbf{0} & \mathbf{0} \\ \mathbf{0} & \mathbf{1}^b_{\uparrow} & \mathbf{0} & \mathbf{0} \\ \mathbf{0} & \mathbf{0} & \mathbf{1}^a_{\downarrow} & \mathbf{0} \\ \mathbf{0} & \mathbf{0} & \mathbf{0} & \mathbf{1}^a_{\uparrow} \end{pmatrix}, \tag{B20}$$

with one nontrivial subblock,

$$\mathbf{G}^{R^t}_{\downarrow} = \begin{pmatrix} e^{-ik_1} & 0 & 0 & \cdots & 0 \\ 0 & 1 & 0 & \cdots & 0 \\ 0 & 0 & 1 & \cdots & 0 \\ \vdots & \vdots & \vdots & \ddots & 0 \\ 0 & 0 & 0 & 0 & 1 \end{pmatrix}, \tag{B21}$$

carrying the gauge for the spin down domain of orbitals b. After the covariant transformation of the glide operator, i.e., $\mathcal{R}^t_{\vec{k}} \to \mathcal{G}^{\mathcal{R}^t\dagger}_{k_1} \mathcal{R}^t_{\vec{k}} \mathcal{G}^{\mathcal{R}^t}_{-k_1}$ and extracting global phase factor we find it dependent only on $k_2/2$ (due to the $\vec{a}_2/2$ shift) in such a way that it eigenvalues are k-independent taking values $g = \pm 1$. The dependence on k_2 of the eigenbasis is such that the eigenvectors with $g = +1$ eigenvalues at fixed k_2 become the $g = -1$ eigenvectors at $k_2 + 2\pi$.

APPENDIX C: HAMILTONIANS AND THEIR SYMMETRY PROPERTIES IN THE GAUGED BASIS

In what follows, we will represent the zigzag Hamiltonians and their symmetries for $L_z = 2,3$ in the basis defined by the gauge transformation $\mathcal{G}_{\vec{k}}$ defined in Sec. B 1. In Sec. C 1, we will show Hamiltonians and their symmetries, including emerging operations in the enlarged BZ, using a very compact Pauli-matrix representation. In Sec. C 2, we demonstrate that in the enlarged BZ, we have to deal with extra reflection and glide operators and in Sec. C 3 we show that the glide blocks of the Hamiltonians in the glide planes are related by a 2π shift. Finally, we will show the special symmetries acting in the parameter space in Sec. C 4.

1. Pauli-matrix representation for $L_z = 2,3$

For zigzag segment lengths $L_z = 2$ and 3, the Hamiltonians are 8×8 and 16×16 Hermitian matrices, respectively. Thus, it is convenient to use the product basis of three and four Pauli matrices to show the exact form of the Hamiltonians and their symmetries in these two cases. For $L_z = 2$, we will decompose the operators in basis of 64 Hermitian matrices whose building blocks are pseudospins $S = 1/2$ defined on three *artificial* sites, i.e.,

$$\begin{aligned} &\sigma^\alpha_1 = \sigma^\alpha \otimes 1_2 \otimes 1_2, \quad \sigma^\alpha_2 = 1_2 \otimes \sigma^\alpha \otimes 1_2, \\ &\sigma^\alpha_3 = 1_2 \otimes 1_2 \otimes \sigma^\alpha, \end{aligned} \tag{C1}$$

with $\alpha = x,y,z$ and σ^α being a Pauli matrix. Hence the Hamiltonian in the gauge transformed basis (in the sense of the gauge transformation of Appendix B 1) and for the shortest

possible zigzag with $L_z = 2$ can be represented as

$$\tilde{\mathcal{H}}_{\tilde{k}} = \sin\frac{k_2}{2}\left(\sin\frac{k_1}{2}\sigma_3^x + \cos\frac{k_1}{2}\sigma_3^y\right)\sigma_1^z\sigma_2^x + \cos\frac{k_2}{2}\left(\sin\frac{k_1}{2}\sigma_3^x - \cos\frac{k_1}{2}\sigma_3^x\right)\sigma_2^x - \cos\frac{k_2}{2}\sigma_3^x - \sin\frac{k_2}{2}\sigma_1^z\sigma_3^y + J_H\sigma_2^z - \lambda\sigma_1^y\sigma_2^z. \quad \text{(C2)}$$

The spatial symmetries take the form

$$\tilde{\mathcal{R}} = \sigma_1^y, \quad \tilde{\mathcal{R}}^t = \sigma_1^y\sigma_3^x, \quad \tilde{\mathcal{I}} = \sigma_3^x, \quad \text{(C3)}$$

and the nonspatial symmetries are

$$\tilde{\mathcal{T}} = \sigma_1^z, \quad \tilde{\mathcal{S}} = \sigma_2^x\sigma_3^z, \quad \tilde{\mathcal{C}} = \sigma_1^z\sigma_2^x\sigma_3^z. \quad \text{(C4)}$$

The algebra is completed by the shift operators defined in the previous section as

$$\chi_1 = \sigma_2^z, \quad \chi_2 = \sigma_3^z. \quad \text{(C5)}$$

It is instructive to check that all these operators really satisfy the relevant relations with respect to the Hamiltonian.

Analogically, for $L_z = 3$, we span a basis of 256 Hermitian matrices whose building blocks are pseudospins $S = 1/2$ acting on four *artificial* sites, i.e.,

$$\sigma_1^\alpha = \sigma^\alpha \otimes 1_2 \otimes 1_2 \otimes 1_2, \quad \sigma_2^\alpha = 1_2 \otimes \sigma^\alpha \otimes 1_2 \otimes 1_2,$$
$$\sigma_3^\alpha = 1_2 \otimes 1_2 \otimes \sigma^\alpha \otimes 1_2, \quad \sigma_4^\alpha = 1_2 \otimes 1_2 \otimes 1_2 \otimes \sigma^\alpha. \quad \text{(C6)}$$

The Hamiltonian in the gauge transformed basis for the zigzag with $L_z = 3$ can be represented as

$$\begin{aligned}\tilde{\mathcal{H}}_{\tilde{k}} = {} & \frac{1}{2}\sin\frac{k_2}{4}\left(\sigma_4^y - \sigma_3^x\sigma_4^y - \sigma_1^z\sigma_3^y\sigma_4^x - \sigma_1^z\sigma_3^z\sigma_4^y\right) + \frac{1}{2}\cos\frac{k_2}{4}\left(-\sigma_4^x - \sigma_3^x\sigma_4^x + \sigma_1^z\sigma_3^y\sigma_4^y + \sigma_1^z\sigma_3^z\sigma_4^x\right) \\ & + \frac{1}{2}\sin\frac{k_2}{4}\sin\frac{k_1}{2}\sigma_2^x\left(\sigma_3^y\sigma_4^y + \sigma_3^z\sigma_4^x + \sigma_1^z\sigma_4^x + \sigma_1^z\sigma_3^x\sigma_4^x\right) + \frac{1}{2}\cos\frac{k_2}{4}\sin\frac{k_1}{2}\sigma_2^x\left(\sigma_3^y\sigma_4^x + \sigma_3^z\sigma_4^y + \sigma_1^z\sigma_4^y - \sigma_1^z\sigma_3^x\sigma_4^y\right) \\ & + \frac{1}{2}\sin\frac{k_2}{4}\cos\frac{k_1}{2}\sigma_1^z\sigma_2^x\left(\sigma_3^y\sigma_4^x + \sigma_3^z\sigma_4^y + \sigma_1^z\sigma_4^y - \sigma_1^z\sigma_3^x\sigma_4^y\right) - \frac{1}{2}\cos\frac{k_2}{4}\cos\frac{k_1}{2}\sigma_1^z\sigma_2^x\left(\sigma_3^y\sigma_4^y + \sigma_3^z\sigma_4^x + \sigma_1^z\sigma_4^x + \sigma_1^z\sigma_3^x\sigma_4^x\right) \\ & + J_H\sigma_2^z - \lambda\sigma_1^y\sigma_2^z. \end{aligned} \quad \text{(C7)}$$

The spatial symmetries take the form

$$\begin{aligned}\tilde{\mathcal{R}} &= \frac{1}{2}\sigma_1^y\left(\left(1-\sigma_3^x\right)\left(1-\sigma_4^z\right) - 2\right), \\ \tilde{\mathcal{R}}^t &= \sigma_1^y\sigma_3^x, \\ \tilde{\mathcal{I}} &= \frac{1}{2}\left(\left(1-\sigma_3^x\right)\left(1+\sigma_4^z\right) - 2\right),\end{aligned} \quad \text{(C8)}$$

and the nonspatial symmetries are

$$\tilde{\mathcal{T}} = \sigma_1^z, \quad \tilde{\mathcal{S}} = \sigma_2^x\sigma_4^z, \quad \tilde{\mathcal{C}} = \sigma_1^z\sigma_2^x\sigma_4^z, \quad \text{(C9)}$$

while the shift operators can be expressed as

$$\chi_1 = \sigma_2^z, \quad \chi_2 = \frac{1}{\sqrt{2}}\sigma_3^z\left(i + \sigma_4^z\right). \quad \text{(C10)}$$

Note that, as expected for $L_z = 3$, $(\chi_2)^4 = 1$, whereas the lower powers are nontrivial, e.g., $(\chi_2)^2 = \sigma_4^z$. Finally, the second- and third-neighbor hopping δ in this basis has a form

$$\tilde{h}(\delta) = \delta\sigma_2^z\sigma_3^x\cos\frac{k_2}{2}. \quad \text{(C11)}$$

One can easily check that it preserves all the symmetries.

2. Multiple glide and reflection operators

An interesting consequence of gauge transformation described in Sec. C 1, related with elongation of Hamiltonian's period, is multiplication of reflection and glide operators. Have a look at the reflection planes, we easily find that for any L_z,

$$[\tilde{\mathcal{H}}_{k_1,0}, \tilde{\mathcal{R}}] = 0, \quad \text{(C12)}$$

but due to the period elongation in $\tilde{\mathcal{H}}_{k_1,k_2}$ we also find that

$$[\tilde{\mathcal{H}}_{k_1,\pi}, \tilde{\mathcal{R}}] \neq 0. \quad \text{(C13)}$$

This means that $k_2 = 0$ is the reflection plane for $\tilde{\mathcal{R}}$ but $k_2 = \pi$ is not. It is not difficult to guess that the second reflection plane should be placed at k_2 equal to half-period of the new BZ, namely at $k_2 = N_\downarrow\pi$. Indeed, we find

$$[\tilde{\mathcal{H}}_{k_1,N_\downarrow\pi}, \tilde{\mathcal{R}}] = 0, \quad \text{(C14)}$$

but one may ask what about $k_2 = \pi, 2\pi, \ldots, (N_\downarrow - 1)\pi$, is there any reflection operator for whom these are the reflection planes? The answer is yes, we can define *shifted* reflection operators $\tilde{\mathcal{R}}_\chi^{(n)}$ in the following way:

$$\tilde{\mathcal{R}}_\chi^{(n)} \equiv \tilde{\mathcal{R}}(\chi_2)^n, \quad \text{(C15)}$$

where $n = 1, 2, \ldots, (N_\downarrow - 1)$. Their action on the Hamiltonian is the following:

$$\tilde{\mathcal{R}}_\chi^{(n)\dagger}\tilde{\mathcal{H}}_{k_1,k_2}\tilde{\mathcal{R}}_\chi^{(n)} = \tilde{\mathcal{H}}_{k_1,-k_2+2\pi n}. \quad \text{(C16)}$$

Now it is easy to notice that

$$\left[\tilde{\mathcal{H}}_{k_1,n\pi}, \tilde{\mathcal{R}}_\chi^{(n)}\right] = \left[\tilde{\mathcal{H}}_{k_1,n\pi+N_\downarrow\pi}, \tilde{\mathcal{R}}_\chi^{(n)}\right] = 0, \quad \text{(C17)}$$

meaning that planes $k_2 = n\pi$ and $k_2 = n\pi + N_\downarrow\pi$ are the reflection planes for the shifted reflection operator $\tilde{\mathcal{R}}_\chi^{(n)}$. Note that unlike initial reflection $\tilde{\mathcal{R}}$ the shifted reflection operators are not Hermitian and unitary, they are only unitary. Similarly, we can define a shifted glide oprator $\tilde{\mathcal{R}}_\chi^t$,

$$\tilde{\mathcal{R}}_\chi^t \equiv \tilde{\mathcal{R}}^t\chi_1. \quad \text{(C18)}$$

Here we have only one shifted operator because for any zigzag $(\chi_1)^2 = 1$. For this operator, the reflection planes are $k_1 = \pi$

and $k_1 = 3\pi$ whereas for nonshifted $\tilde{\mathcal{R}}^t$ these are $k_1 = 0$ and $k_1 = 2\pi$. Note that the period of gauged Hamiltonian $\tilde{\mathcal{H}}_{k_1,k_2}$ in k_1 is 4π for any L_z. By taking products of shifted reflection and glide operators we can construct different shifted inversion operators for different inversion points in the enlarged BZ of $\tilde{\mathcal{H}}_{k_1,k_2}$. The final conclusion for this section is that, however, the k-dependence in spatial symmetry operators can be removed by a proper gauge transformation, this dependence reappears in the gauged basis as a multiple definition of these operators for different symmetry-invariant k points.

3. Shift equivalence of the glide blocks of the Hamiltonian

In this section, we will focus on Hamiltonian in its glide planes. From Sec. C 2, we know that in the gauged basis we should cosider two glide operators, $\tilde{\mathcal{R}}^t$ and the shifted one $\tilde{\mathcal{R}}^t_\chi$, for glide planes $k_1 = 0$ and π. Looking into Sec. C 1, we see that both for $L_z = 2$ and $L_z = 3$ these operators anticommute with shift operators χ_2, i.e.,

$$\{\tilde{\mathcal{R}}^t, \chi_2\} = 0, \quad \{\tilde{\mathcal{R}}^t_\chi, \chi_2\} = 0, \tag{C19}$$

and the same property holds for any other L_z. Now, take the eigenbasis $\mathcal{V}$ of $\tilde{\mathcal{R}}^t$ or $\tilde{\mathcal{R}}^t_\chi$ and write the two glide plane Hamiltonians as

$$\tilde{\mathcal{H}}'_{0(\pi),k_2} \equiv \tilde{\mathcal{V}}^\dagger \tilde{\mathcal{H}}_{0(\pi),k_2} \tilde{\mathcal{V}} = \begin{pmatrix} \tilde{H}^+_{0(\pi),k_2} & 0 \\ 0 & \tilde{H}^-_{0(\pi),k_2} \end{pmatrix}, \tag{C20}$$

where $\tilde{H}^\pm_{0(\pi),k_2}$ denote the blocks of equal size in the subspaces of $+1$ and -1 eigenvalues of $\tilde{\mathcal{R}}^t$ or $\tilde{\mathcal{R}}^t_\chi$ operators. In the same basis, we find χ_2 in the antidiagonal form of

$$\chi'_2 \equiv \mathcal{V}^\dagger \chi_2 \mathcal{V} = \begin{pmatrix} 0 & \xi_2 \\ \xi_2 & 0 \end{pmatrix}, \tag{C21}$$

where ξ_2 is a unitary matrix. From the relation of shift operator with respect to the Hamiltonian, namely,

$$\chi_2'^\dagger \tilde{\mathcal{H}}'_{0(\pi),k_2} \chi'_2 = \tilde{\mathcal{H}}'_{0(\pi),k_2+2\pi}, \tag{C22}$$

we find that

$$\xi_2^\dagger \tilde{H}^\mp_{0(\pi),k_2} \xi_2 = \tilde{H}^\pm_{0(\pi),k_2+2\pi}. \tag{C23}$$

This a major result that shows that the glide plane Hamiltonian for $+1$ gliding eigenstates at quasimomentum k_2 is related with the Hamiltonian for -1 gliding eignestates at point $k_2 + 2\pi$ only by a basis rotation. What more, if we remove the gauging and come back to original basis we find that these two block are equal,

$$H^\mp_{0(\pi),k_2} = H^\pm_{0(\pi),k_2+2\pi}. \tag{C24}$$

Note that 2π shift in k_2 is relevant from the point of view of $H^\mp_{0(\pi),k_2}$ because now we are in the eigenbasis of $\mathcal{R}^t_{k_1,k_2}$ which is k-dependent and the period of $H^\mp_{0(\pi),k_2}$ is elongated. This property, which holds for any zigzag segment length L_z, implies that the whole spectrum of the glide-plane Hamiltonian is fully determined in just one eigensubspace of the glide operator.

4. Symmetries in the parameters space

For any zigzag segment length L_z, it is possible to find additional symmetries that can be associated to two reflections operators $\tilde{\mathcal{X}}$ and $\tilde{\mathcal{Y}}$ and an inversion $\tilde{\mathcal{Z}} = \tilde{\mathcal{X}}\tilde{\mathcal{Y}}$ that act uniquely in the parameters space (J_H, λ). The reflections are active only in the glide plane $k_1 = 0$ and satisfy the relations,

$$\begin{aligned} \tilde{\mathcal{X}}^\dagger \tilde{\mathcal{H}}_{0,k_2}(J_H,\lambda)\tilde{\mathcal{X}} &= \tilde{\mathcal{H}}_{0,k_2}(\lambda, J_H), \\ \tilde{\mathcal{Y}}^\dagger \tilde{\mathcal{H}}_{0,k_2}(J_H,\lambda)\tilde{\mathcal{Y}} &= \tilde{\mathcal{H}}_{0,k_2}(-\lambda, -J_H). \end{aligned} \tag{C25}$$

Thus we see that the reflection planes in the parameters plane (J_H, λ) are in the direction $J_H = \lambda$ and $J_H = -\lambda$. The action of the inversion $\tilde{\mathcal{Z}}$ on the Hamiltonian is obviously

$$\tilde{\mathcal{Z}}^\dagger \tilde{\mathcal{H}}_{0,k_2}(J_H,\lambda)\tilde{\mathcal{Z}} = \tilde{\mathcal{H}}_{0,k_2}(-J_H, -\lambda). \tag{C26}$$

The general matrix form of the two reflections in the gauged basis is

$$\tilde{\mathcal{X}} = \frac{1}{2}\begin{pmatrix} \mathbf{1}_{N_\downarrow} & -\mathbf{1}_{N_\downarrow} & i\mathbf{1}_{N_\downarrow} & i\mathbf{1}_{N_\downarrow} \\ -\mathbf{1}_{N_\downarrow} & \mathbf{1}_{N_\downarrow} & i\mathbf{1}_{N_\downarrow} & i\mathbf{1}_{N_\downarrow} \\ -i\mathbf{1}_{N_\downarrow} & -i\mathbf{1}_{N_\downarrow} & \mathbf{1}_{N_\downarrow} & -\mathbf{1}_{N_\downarrow} \\ -i\mathbf{1}_{N_\downarrow} & -i\mathbf{1}_{N_\downarrow} & -\mathbf{1}_{N_\downarrow} & \mathbf{1}_{N_\downarrow} \end{pmatrix} \tag{C27}$$

and

$$\tilde{\mathcal{Y}} = -\frac{1}{2}\begin{pmatrix} -\mathbf{1}_{N_\downarrow} & \mathbf{1}_{N_\downarrow} & i\mathbf{1}_{N_\downarrow} & i\mathbf{1}_{N_\downarrow} \\ \mathbf{1}_{N_\downarrow} & -\mathbf{1}_{N_\downarrow} & i\mathbf{1}_{N_\downarrow} & i\mathbf{1}_{N_\downarrow} \\ -i\mathbf{1}_{N_\downarrow} & -i\mathbf{1}_{N_\downarrow} & -\mathbf{1}_{N_\downarrow} & \mathbf{1}_{N_\downarrow} \\ -i\mathbf{1}_{N_\downarrow} & -i\mathbf{1}_{N_\downarrow} & \mathbf{1}_{N_\downarrow} & -\mathbf{1}_{N_\downarrow} \end{pmatrix}. \tag{C28}$$

Note that the spectra of $\tilde{\mathcal{X}}$ and $\tilde{\mathcal{Y}}$ are the same and consist of $N_\downarrow$ eigenvalues -1 and $3N_\downarrow$eigenvalues 1, which coincides with the spectrum of the SU(2) spin interchange operator $X_{12} = \frac{1}{2}(1 + \vec{\sigma}_1\vec{\sigma}_2)$ taken $N_\downarrow$ times. The spectrum of $\tilde{\mathcal{Z}}$ consist of equal number of $+1$ and -1 eigenvalues.

For $L_z = 2$ and 3 operators, $\tilde{\mathcal{X}}$, $\tilde{\mathcal{Y}}$ and $\tilde{\mathcal{Z}}$ can be written in terms Pauli matrices (C1) or (C6) as

$$\begin{aligned} \tilde{\mathcal{X}} &= \frac{1}{2}\left(1 - \sigma_1^y - \sigma_1^y\sigma_2^x - \sigma_2^x\right), \\ \tilde{\mathcal{Y}} &= -\sigma_2^x\tilde{\mathcal{X}}, \\ \tilde{\mathcal{Z}} &= -\sigma_2^x. \end{aligned} \tag{C29}$$

For these two shortest zigzags with $L_z = 2$ and 3, we find that the inversion operator $\tilde{\mathcal{Z}}$ satisfies

$$\tilde{\mathcal{Z}}^\dagger \tilde{\mathcal{H}}_{k_1,k_2}(J_H,\lambda)\tilde{\mathcal{Z}} = \tilde{\mathcal{H}}_{k_1,k_2}(-J_H, -\lambda), \tag{C30}$$

for any k point, whereas only for $L_z = 2$, we get extra relations for the $\tilde{\mathcal{X}}$ and $\tilde{\mathcal{Y}}$ operators in the plane $k_2 = 0$,

$$\begin{aligned} \tilde{\mathcal{X}}^\dagger \tilde{\mathcal{H}}_{k_1,0}(J_H,\lambda)\tilde{\mathcal{X}} &= \tilde{\mathcal{H}}_{k_1,0}(\lambda, J_H), \\ \tilde{\mathcal{Y}}^\dagger \tilde{\mathcal{H}}_{k_1,0}(J_H,\lambda)\tilde{\mathcal{Y}} &= \tilde{\mathcal{H}}_{k_1,0}(-\lambda, -J_H). \end{aligned} \tag{C31}$$

APPENDIX D: DETERMINANT EQUIVALENCE OF THE GLIDE BLOCKS

In the following two sections, we will demonstrate a mechanism related with the existence of nonunitary symmetries that lead to the 2π-shift invariance of the determinants of the glide blocks of the $z3$ Hamiltonian. In Sec. D 1, we show this

property at half filling or $\mu = 0$ and in Sec. D 2 at special $\mu = \mu_0 > 0$. For $\mu = 0$, we note that the 2π-shift invariance seems to exist for any L_z.

1. Half-filling case

In the previous section, we showed that the glide blocks of the Hamiltonian are related by a 2π shift as

$$H^{\mp}_{0(\pi),k_2} = H^{\pm}_{0(\pi),k_2+2\pi}. \tag{D1}$$

Now we will show that at *the same* k_2 the spectra of $H^{\mp}_{0(\pi),k_2}$ are related in a very special way. Namely, for any L_z and $k_1 = 0$, we find that

$$\det H^{+}_{0,k_2} \equiv \det H^{-}_{0,k_2} \equiv \det H^{+}_{0,k_2+2\pi}, \tag{D2}$$

and for any *odd* L_z and $k_1 = \pi$, we have

$$\det H^{+}_{\pi,k_2} \equiv \det H^{-}_{\pi,k_2} \equiv \det H^{+}_{\pi,k_2+2\pi}. \tag{D3}$$

This means that in each block the product of all eigenvalues is 2π periodic although these eigenvalues by themselves have longer period.

Let us show why such property of determinant holds by considering zigzag patterns with $L_z = 3$ and $k_1 = 0$. We find the determinant of a glide block to be

$$\det H^{+}_{0,k_2} = \left(-2 + \left(J_H^2 - \lambda^2\right)^2 + 2\cos k_2\right)^2, \tag{D4}$$

although the periodicity of H^{+}_{0,k_2} is 4π.

Such relation is related to a sort of *hidden* symmetry. Indeed, the block can be written in the following way:

$$H^{+}_{0,k_2} = h_{k_2} + \bar{H}_{k_2}, \tag{D5}$$

where $\bar{H}_{k_2}$ is the 2π periodic part of H^{+}_{0,k_2}, i.e., $\bar{H}_{k_2+2\pi} \equiv \bar{H}_{k_2}$ and h_{k_2} is the part with 4π period. Since the dependence on k_2 is always enclosed in sine and cosine type functions we have

$$h_{k_2+2\pi} \equiv -h_{k_2}. \tag{D6}$$

Now, we can write the desired determinant in the following way,

$$\det H^{+}_{0,k_2} = \det\left(h_{k_2} + \bar{H}_{k_2}\right) = \det h_{k_2} \det\left(1 + \Sigma_{k_2}\right), \tag{D7}$$

where $\Sigma_{k_2} \equiv h^{-1}_{k_2}\bar{H}_{k_2}$. This step requires h_{k_2} to be an invertible function, and it holds because h_{k_2} has eigenvalues $\pm\lambda$ so it is nonsingular for any k_2. The new operator Σ_{k_2} satisfies the relation $\Sigma_{k_2+2\pi} \equiv -\Sigma_{k_2}$. It is non-Hermitian and in principle can be nondiagonalizable. our case, we find Σ_{k_2} to be diagonalizable and its spectrum to be chiral with the following eigenvalues:

$$s_{k_2} = \pm\frac{1}{\lambda}\sqrt{J_H^2 \pm 2\sin\frac{k_2}{2}}, \tag{D8}$$

and being double degenerate. This means that there exist a nonsingular operator β_{k_2} that anticommutes with Σ_{k_2} namely

$$\left\{\beta_{k_2}, \Sigma_{k_2}\right\} \equiv 0. \tag{D9}$$

Using this property, we can prove that determinant of H^{+}_{0,k_2} is 2π periodic as

$$\det H^{+}_{0,k_2+2\pi} = (-1)^{N_\downarrow} \det h_{k_2} \det(1 - \Sigma_{k_2}). \tag{D10}$$

Then, we focus on the second term and the anticommutation of β_{k_2},

$$\det\left(1 - \beta^{-1}_{k_2}\beta_{k_2}\Sigma_{k_2}\right) = \det\left(1 + \beta^{-1}_{k_2}\Sigma_{k_2}\beta_{k_2}\right),$$

as well as we take into account the Silvester identity that sets the relation between the determinants of two generic matrices A and B:

$$\det(1 + AB) = \det(1 + BA). \tag{D11}$$

Choosing $A = \beta^{-1}_{k_2}\Sigma_{k_2}$ and $B = \beta_{k_2}$ we finally have that

$$\det\left(1 + \beta^{-1}_{k_2}\Sigma_{k_2}\beta_{k_2}\right) = \det(1 + \Sigma_{k_2}), \tag{D12}$$

and thus

$$\det(1 - \Sigma_{k_2}) = \det(1 + \Sigma_{k_2}). \tag{D13}$$

This implies that

$$\det H^{+}_{0,k_2+2\pi} = (-1)^{N_\downarrow} \det H^{+}_{0,k_2}. \tag{D14}$$

Since $N_\downarrow$ is always even in our zigzag patterns we succeed in demonstrating that the determinant of the glide block is indeed 2π periodic. We point out that a crucial ingredient for the proof is given by the existence of an *invertible* operator β_{k_2} that anticommutes with Σ_{k_2}. We found that such chirality also occurs for $k = \pi$ glide plane and for other zigzag segment lengths L_z.

2. Away from half-filling

The property of determinat of a glide block described in the previous section can be more general in case of some L_z. Namely, we can find such values of chemical potential μ that a following relation is satisfied:

$$\det\left(H^{+}_{0,k_2} - \mu\right) \equiv \det\left(H^{+}_{0,k_2+2\pi} - \mu\right). \tag{D15}$$

In case of zigzag $L_z = 3$, we find that there is one nontrivial value of μ satisfying this relation

$$\mu_0 = \pm\sqrt{2 + J_H^2 + \lambda^2}, \tag{D16}$$

where the freedom of sign comes from the chirality of H^{+}_{0,k_2}. The determinant then becomes

$$\det\left(H^{+}_{0,k_2} - \mu_0\right) = 4\left(1 - 2J_H^2\lambda^2 + \cos k_2\right)^2. \tag{D17}$$

So indeed it is 2π periodic. Why it happens, we can prove in a indirect way. We define a chiral-square block $H^{+(2)}_{0,k_2}$ as

$$H^{+(2)}_{\mu,k_2} \equiv \left(H^{+}_{0,k_2}\right)^2 - \mu^2. \tag{D18}$$

For this block, we can prove using the method from the previous section that

$$\det H^{+(2)}_{\mu,k_2} = \det H^{+(2)}_{\mu,k_2+2\pi}. \tag{D19}$$

Now having this we can relate the determinant of $H^{+(2)}_{\mu,k_2}$ with determinant of $(H^{+}_{0,k_2} - \mu)$ (modulo sign) in a following way:

$$\begin{aligned}\det H^{+(2)}_{\mu,k_2} &= \det\left(H^{+}_{0,k_2} + \mu\right)\det\left(H^{+}_{0,k_2} - \mu\right)\\ &= (-1)^{N_\downarrow}\det\left(H^{+}_{0,k_2} - \mu\right)^2,\end{aligned} \tag{D20}$$

where for the second equality we used the chirality operator of H^{+}_{0,k_2} and the Silvester identity of Eq. (D11) in the same way as we did in previous section for Σ_{k_2} and β_{k_2}.

The prove of property (D19) can be done in way described in the previous section. First, we decompose $H^{+(2)}_{\mu,k_2}$,

$$H^{+(2)}_{\mu,k_2} = h^{(2)}_{k_2} + \bar{H}^{(2)}_{\mu,k_2}, \tag{D21}$$

into the part which is 2π periodic $\bar{H}^{(2)}_{\mu,k_2}$ and the rest, $h^{(2)}_{k_2}$ satisfying $h^{(2)}_{k_2+2\pi} \equiv -h^{(2)}_{k_2}$. Now we define the operator $\Sigma^{(2)}_{\mu,k_2}$, which we would like to be chiral, i.e.,

$$\Sigma^{(2)}_{\mu,k_2} \equiv h^{(2)-1}_{k_2} \bar{H}^{(2)}_{\mu,k_2}. \tag{D22}$$

Indeed, the spectrum of $\Sigma^{(2)}_{\mu,k_2}$ is chiral if only $\mu = \mu_0$ but there is one subtlety here $\Sigma^{(2)}_{\mu_0,k_2}$ is nondiagonalizable (defective). We find that it has a nontrivial Jordan form given by

$$\Sigma^{(2)'}_{\mu_0,k_2} = \begin{pmatrix} -s_{k_2} & 1 & 0 & 0 & 0 & 0 & 0 & 0 \\ 0 & -s_{k_2} & 0 & 0 & 0 & 0 & 0 & 0 \\ 0 & 0 & -s_{k_2} & 1 & 0 & 0 & 0 & 0 \\ 0 & 0 & 0 & -s_{k_2} & 0 & 0 & 0 & 0 \\ 0 & 0 & 0 & 0 & s_{k_2} & 0 & 0 & 0 \\ 0 & 0 & 0 & 0 & 0 & s_{k_2} & 0 & 0 \\ 0 & 0 & 0 & 0 & 0 & 0 & s_{k_2} & 0 \\ 0 & 0 & 0 & 0 & 0 & 0 & 0 & s_{k_2} \end{pmatrix}, \tag{D23}$$

with eigenvalues

$$\pm s_{k_2} \equiv \pm \frac{1}{J_H \lambda} \cos \frac{k_2}{2}, \tag{D24}$$

and where $\Sigma^{(2)'}_{\mu_0,k_2}$ is related with $\Sigma^{(2)}_{\mu_0,k_2}$ by a similarity transformation,

$$\Sigma^{(2)'}_{\mu_0,k_2} = \gamma^{-1} \Sigma^{(2)}_{\mu_0,k_2} \gamma. \tag{D25}$$

The fact that $\Sigma^{(2)}_{\mu_0,k_2}$ is defective means that we cannot find a nonsingular matrix $\beta^{(2)}_{\mu_0,k_2}$ that anticommutes with $\Sigma^{(2)}_{\mu_0,k_2}$ eventhough its spectrum is chiral. This is, however, not a big complication because the nondiagonal entries in $\Sigma^{(2)'}_{\mu_0,k_2}$ do not affect the determinant of $(1 + \Sigma^{(2)'}_{\mu_0,k_2})$, which is important for the proof. Hence we can replace $\Sigma^{(2)}_{\mu_0,k_2}$ by a new operator $\bar{\Sigma}^{(2)}_{\mu_0,k_2}$ whose form in the basis given by γ is purely diagonal and is identical to $\Sigma^{(2)'}_{\mu_0,k_2}$ without nondiagonal entries. For this operator, one can find an anticommuting and nonsingular partner and thus the proof is complete.

[1] M. Z. Hasan and C. L. Kane, Rev. Mod. Phys. **82**, 3045 (2010).
[2] X.-L. Qi and S.-C. Zhang, Rev. Mod. Phys. **83**, 1057 (2011).
[3] C.-K. Chiu, J. C. Y. Teo, A. P. Schnyder, and S. Ryu, Rev. Mod. Phys. **88**, 035005 (2016).
[4] H. M. Weng, R. Yu, X. Hu, X. Dai, and Z. Fang, Adv. Phys. **64**, 227 (2015).
[5] C. L. Kane and E. J. Mele, Phys. Rev. Lett. **95**, 146802 (2005).
[6] B. A. Bernevig, T. L. Hughes, and S.-C. Zhang, Science **314**, 1757 (2006).
[7] J. E. Moore and L. Balents, Phys. Rev. B **75**, 121306 (2007).
[8] L. Fu, C. L. Kane, and E. J. Mele, Phys. Rev. Lett. **98**, 106803 (2007).
[9] M. König *et al.*, Science **318**, 766 (2007).
[10] D. Hsieh *et al.*, Nature **452**, 970 (2008).
[11] Y. Xia *et al.*, Nature Phys. **5**, 398 (2009).
[12] G. E. Volovik, *The Universe in a Helium Droplet* (Clarendon, Oxford, 2003).
[13] G. E. Volovik, Lect. Notes Phys. **718**, 31 (2007).
[14] X. Wan, A. M. Turner, A. Vishwanath, and S. Y. Savrasov, Phys. Rev. B **83**, 205101 (2011).
[15] T. Heikkil and G. E. Volovik, JETP Lett. **93**, 59 (2011).
[16] K.-Y. Yang, Y.-M. Lu, and Y. Ran, Phys. Rev. B **84**, 075129 (2011).
[17] A. A. Burkov and L. Balents, Phys. Rev. Lett. **107**, 127205 (2011).
[18] W. Witczak-Krempa and Y.-B. Kim, Phys. Rev. B **85**, 045124 (2012).
[19] G. Xu, H. Weng, Z. Wang, X. Dai, and Z. Fang, Phys. Rev. Lett. **107**, 186806 (2011).
[20] G. B. Halász and L. Balents, Phys. Rev. B **85**, 035103 (2012).
[21] H. Weng, C. Fang, Z. Fang, B. A. Bernevig, and X. Dai, Phys. Rev. X **5**, 011029 (2015).
[22] S.-M. Huang, S.-Y. Xu, I. Belopolski, C.-C. Lee, G. Chang, B. Wang, N. Alidoust, G. Bian, M. Neupane, C. Zhang, S. Jia, A. Bansil, H. Lin, and M. Z. Hasan, Nat. Commun. **6**, 7373 (2015).

[23] S.-Y. Xu *et al.*, Science **349**, 613 (2015).
[24] M. Imada, A. Fujimori, and Y. Tokura, Rev. Mod. Phys. **70**, 1039 (1998).
[25] Y. Tokura and N. Nagaosa, Science **288**, 462 (2000).
[26] A. M. Oleś, J. Phys.: Condens. Matter **24**, 313201 (2012).
[27] M. Vojta, Adv. Phys. **58**, 699 (2009).
[28] W. Brzezicki, A. M. Oleś, and M. Cuoco, Phys. Rev. X **5**, 011037 (2015).
[29] W. Brzezicki, M. Cuoco, and A. M. Oleś, J. Supercond. Novel Magn. **29**, 563 (2016).
[30] B. Q. Lv, H. M. Weng, B. B. Fu, X. P. Wang, H. Miao, J. Ma, P. Richard, X. C. Huang, L. X. Zhao, G. F. Chen, Z. Fang, X. Dai, T. Qian, and H. Ding, Phys. Rev. X **5**, 031013 (2015).
[31] B. Q. Lv, N. Xu, H. M. Weng, J. Z. Ma, P. Richard, X. C. Huang, L. X. Zhao, G. F. Chen, C. E. Matt, F. Bisti, V. N. Strocov, J. Mesot, Z. Fang, X. Dai, T. Qian, M. Shi, and H. Ding, Nat. Phys. **11**, 724 (2015).
[32] S.-Y. Xu, C. Liu, S. K. Kushwaha, R. Sankar, J. W. Krizan, I. Belopolski, M. Neupane, G. Bian, N. Alidoust, T.-R. Chang, H.-T. Jeng, C.-Y. Huang, W.-F. Tsai, H. Lin, P. P. Shibayev, F.-C. Chou, R. J. Cava, and M. Z. Hasan, Science **347**, 294 (2015).
[33] W. Brzezicki, C. Noce, A. Romano, and M. Cuoco, Phys. Rev. Lett. **114**, 247002 (2015).
[34] S. Biermann, L. de Medici, and A. Georges, Phys. Rev. Lett. **95**, 206401 (2005).
[35] J. Rincoón, A. Moreo, G. Alvarez, and E. Dagotto, Phys. Rev. Lett. **112**, 106405 (2014).
[36] C. J. Bradley and A. P. Cracknell, *The Mathematical Theory of Symmetry in Solids* (Clarendon, Oxford, 1972).
[37] Y. Tokura, Rep. Prog. Phys. **69**, 797 (2006).
[38] A. Muoz, M. T. Casáis, J. A. Alonso, M. J. Martínez-Lope, J. L. Martínez, and M. T. Fernández-Díaz, Inorg. Chem. **40**, 1020 (2001).
[39] S. Dong, J.-M. Liu, S. W. Cheong, and Z. F. Ren, Adv. Phys. **64**, 519 (2015).
[40] J. E. Ortmann, J. Y. Liu, J. Hu, M. Zhu, J. Peng, M. Matsuda, X. Ke, and Z. Q. Mao, Sci. Rep. **3**, 2950 (2013).
[41] R. Mathieu, A. Asamitsu, Y. Kaneko, J. P. He, X. Z. Yu, R. Kumai, Y. Onose, N. Takeshita, T. Arima, H. Takagi, and Y. Tokura, Phys. Rev. B **72**, 092404 (2005).
[42] M. A. Hossain *et al.*, Phys. Rev. B **86**, 041102(R) (2012).
[43] D. Mesa, F. Ye, S. Chi, J. A. Fernandez-Baca, W. Tian, B. Hu, R. Jin, E. W. Plummer, and J. Zhang, Phys. Rev. B **85**, 180410(R) (2012).
[44] Y. Xia, D. Qian, L. Wray, D. Hsieh, G. F. Chen, J. L. Luo, N. L. Wang, and M. Z. Hasan, Phys. Rev. Lett. **103**, 037002 (2009).
[45] G. F. Chen, Z. G. Chen, J. Dong, W. Z. Hu, G. Li, X. D. Zhang, P. Zheng, J. L. Luo, and N. L. Wang, Phys. Rev. B **79**, 140509(R) (2009).
[46] D. Fobes, I. A. Zaliznyak, Z. Xu, R. Zhong, G. Gu, J. M. Tranquada, L. Harriger, D. Singh, V. O. Garlea, M. Lumsden, and B. Winn, Phys. Rev. Lett. **112**, 187202 (2014).
[47] F. Ye, S. Chi, H. Cao, B. C. Chakoumakos, J. A. Fernandez-Baca, R. Custelcean, T. F. Qi, O. Korneta, and G. Cao, Phys. Rev. B **85**, 180403 (2012).
[48] S. K. Choi, R. Coldea, A. N. Kolmogorov, T. Lancaster, I. I. Mazin, S. J. Blundell, P. G. Radaelli, Y. Singh, P. Gegenwart, K. R. Choi, S.-W. Cheong, P. J. Baker, C. Stock, and J. Taylor, Phys. Rev. Lett. **108**, 127204 (2012).
[49] J. L. García-Munoz, J. Rodríguez-Carvajal, and P. Lacorre, Phys. Rev. B **50**, 978 (1994).
[50] J. A. Alonso *et al.*, Phys. Rev. Lett. **82**, 3871 (1999).
[51] M. T. Fernández-Díaz, J. A. Alonso, M. J. Martinez-Lope, M. T. Casais, and J. L. Garcia-Munoz, Phys. Rev. B **64**, 144417 (2001).
[52] J.-S. Zhou, J. B. Goodenough, and B. Dabrowski, Phys. Rev. Lett. **95**, 127204 (2005).
[53] R. S. K. Mong, A. M. Essin, and J. E. Moore, Phys. Rev. B **81**, 245209 (2010).
[54] C.-X. Liu, R.-X. Zhang, and B. K. VanLeeuwen, Phys. Rev. B **90**, 085304 (2014).
[55] C. Fang and L. Fu, Phys. Rev. B **91**, 161105 (2015).
[56] K. Shiozaki, M. Sato, and K. Gomi, Phys. Rev. B **91**, 155120 (2015).
[57] X.-Y. Dong and C.-X. Liu, Phys. Rev. B **93**, 045429 (2016).
[58] Q.-Z. Wang and C.-X. Liu, Phys. Rev. B **93**, 020505 (2016).
[59] D. Varjas, F. de Juan, and Y.-M. Lu, Phys. Rev. B **92**, 195116 (2015).
[60] S. Sahoo, Z. Zhang, and J. C. Y. Teo, Phys. Rev. B **94**, 165142 (2016).
[61] L. Lu, C. Fang, L. Fu, S. G. Johnson, J. D. Joannopoulos, and M. Soljačić, Nat. Phys. **12**, 337 (2016).
[62] K. Shiozaki, M. Sato, and K. Gomi, Phys. Rev. B **93**, 195413 (2016).
[63] S. Kobayashi, Y. Yanase, and M. Sato, Phys. Rev. B **94**, 134512 (2016).
[64] A. Alexandradinata, Z. Wang, and B. A. Bernevig, Phys. Rev. X **6**, 021008 (2016).
[65] P.-Y. Chang, O. Erten, and P. Coleman, arXiv:1603.03435.
[66] Z. Wang, A. Alexandradinata, R. J. Cava, and B. A. Bernevig, Nature (London) **532**, 189 (2016).
[67] S. A. Parameswaran, A. M. Turner, D. P. Arovas, and A. Vishwanath, Nat. Phys. **9**, 299 (2013).
[68] H. Watanabe, H. C. Po, A. Vishwanath, and M. Zaletel, Proc. Natl. Acad. Sci. USA **112**, 14551 (2015).
[69] S. M. Young and C. L. Kane, Phys. Rev. Lett. **115**, 126803 (2015).
[70] H. Watanabe, H. C. Po, M. P. Zaletel, and A. Vishwanath, Phys. Rev. Lett. **117**, 096404 (2016).
[71] Q.-F. Liang, J. Zhou, R. Yu, Z. Wang, and H. Weng, Phys. Rev. B **93**, 085427 (2016).
[72] J. W. F. Venderbos, Phys. Rev. B **93**, 115107 (2016).
[73] B.-J. Yang, T. A. Bojesen, T. Morimoto, and A. Furusaki, Phys. Rev. B **95**, 075135 (2017).
[74] L Muechler, A. Alexandradinata, T. Neupert, and R. Cava, Phys. Rev. X **6**, 041069 (2016).
[75] Y. X. Zhan and A. P. Schnyder, Phys. Rev. B **94**, 195109 (2016).
[76] B. J. Wieder and C. L. Kane, Phys. Rev. B **94**, 155108 (2016).
[77] J. H. Pixley, S. Lee, B. Brandom, S. A. Parameswaran, arXiv:1609.04023.
[78] T. Bzduşek, Q. Wu, A. Rüegg, M. Sigrist, and A. A. Soluyanov, Nature **538**, 75 (2016).
[79] B. J. Wieder, Y. Kim, A. M. Rappe, and C. L. Kane, Phys. Rev. Lett. **116**, 186402 (2016).
[80] B. Bradlyn, J. Cano, Z. Wang, M. G. Vergniory, C. Felser, R. J. Cava, and B. A. Bernevig, arXiv:1603.03093.
[81] Y. Chen, H.-S. Kim, and H.-Y. Kim, Phys. Rev. B **93**, 155140 (2016).
[82] A. Altland and M. R. Zirnbauer, Phys. Rev. B **55**, 1142 (1997).

[83] C.-K. Chiu and A. P. Schnyder, Phys. Rev. B **90**, 205136 (2014).
[84] Y. X. Zhao and Z. D. Wang, Phys. Rev. Lett. **110**, 240404 (2013); Phys. Rev. B **89**, 075111 (2014)
[85] A. Alexandradinata, Xi Dai, and B. Andrei Bernevig, Phys. Rev. B **89**, 155114 (2014)
[86] Y. Li, S. Dong, and S.-P. Kou, Phys. Rev. B **93**, 085139 (2016).
[87] L. Brey and P. B. Littlewood, Phys. Rev. Lett. **95**, 117205 (2005).
[88] K. Du *et al.*, Nat. Comm. **6**, 6179 (2015).
[89] Y. X. Zhao, A. P. Schnyder, and Z. D. Wang, Phys. Rev. Lett. **116**, 156402 (2016).